Since January 2020 Elsevier has created a COVID-19 resource centre with free information in English and Mandarin on the novel coronavirus COVID-19. The COVID-19 resource centre is hosted on Elsevier Connect, the company's public news and information website.

European Journal of Medicinal Chemistry 257 (2023) 115512

Contents lists available at ScienceDirect

European Journal of Medicinal Chemistry

journal homepage: www.elsevier.com/locate/ejmech

Research paper

Design, synthesis and biological evaluation of peptidomimetic benzothiazolyl ketones as 3CL^{pro} inhibitors against SARS-CoV-2

Hanxi Yang [a,b,1], Mengyuan You [c,1], Xiaoyang Shu [d,1], Jingyao Zhen [b,e], Mengwei Zhu [f,g], Tiantian Fu [f,g], Yan Zhang [b], Xiangrui Jiang [b,e], Leike Zhang [d,h], Yechun Xu [b,c], Yumin Zhang [d,***], Haixia Su [b,**], Qiumeng Zhang [b,*], Jingshan Shen [b]

[a] College of Chemistry, Zhengzhou University, 100 Kexuedadao Road, Zhengzhou, 450001, China
[b] State Key Laboratory of Drug Research, Shanghai Institute of Materia Medica, Chinese Academy of Sciences, Shanghai, 201203, China
[c] School of Chinese Materia Medica, Nanjing University of Chinese Medicine, Nanjing, 210023, China
[d] State Key Laboratory of Virology, Wuhan Institute of Virology, Center for Biosafety Mega-Science, Chinese Academy of Sciences, Wuhan, Hubei, 430071, China
[e] University of Chinese Academy of Sciences, No. 19A Yuquan Road, Beijing, 100049, PR China
[f] College of Pharmacy, An Hui University of Traditional Chinese Medicine, Hefei, 230012, China
[g] Yangtze Delta Drug Advanced Research Institute and Yangtze Delta Pharmaceutical College, Nantong, 226133, China
[h] Hubei Jiangxia Laboratory, Wuhan, 430200, China

ARTICLE INFO

Keywords:
Peptidomimetics
Benzothiazolyl ketone
3CL^{pro} inhibitor
Pharmacokinetic properties
SARS-CoV-2

ABSTRACT

A series of peptidomimetic compounds containing benzothiazolyl ketone and [2.2.1] azabicyclic ring was designed, synthesized and evaluated in the hope of obtaining potent oral 3CL^{pro} inhibitors with improved pharmacokinetic properties. Among the target compounds, **11b** had the best enzymatic potency (IC_{50} = 0.110 μM) and **11e** had the best microsomal stability ($t_{1/2}$ > 120 min) and good enzyme activity (IC_{50} = 0.868 μM). Therefore, compounds **11b** and **11e** were chosen for further evaluation of pharmacokinetics in ICR mice. The results exhibited that the $AUC_{(0-t)}$ of **11e** was 5143 h*ng/mL following single-dose oral administration of 20 mg/kg, and the F was 67.98%. Further structural modification was made to obtain compounds **11g**-**11j** based on **11e**. Among them, **11j** exhibited the best enzyme inhibition activity against SARS-CoV-2 3CL^{pro} (IC_{50} = 1.646 μM), the $AUC_{(0-t)}$ was 32473 h*ng/mL (20 mg/kg, po), and the F was 48.1%. In addition, **11j** displayed significant anti-SARS-CoV-2 activity (EC_{50} = 0.18 μM) and low cytotoxicity (CC_{50} > 50 μM) in Vero E6 cells. All of the above results suggested that compound **11j** was a promising lead compound in the development of oral 3CL^{pro} inhibitors and deserved further research.

1. Introduction

COVID-19 is an acute respiratory infectious disease caused by the severe acute respiratory syndrome coronavirus 2 (SARS-CoV-2) which has engendered a huge threat to the global economy and public health [1,2]. The ORF1a and ORF1b genes account for about 2/3 of the total length of the SARS-CoV-2 genome and encode two polyproteins [3,4]. The two polyproteins can be cleaved by 3C-like protease (3CL^{pro}) and Papain-like protease (PL^{pro}) to form sixteen functional proteins [5,6]. It is worth mentioning that 3CL^{pro} is responsible for the cleavage of 11 sites on polyproteins and plays an essential role in viral replication and propagation [7,8]. Besides, it has been proven that the catalytic domains of different coronaviruses 3CL^{pro} are highly conservative, thus 3CL^{pro} inhibitors may have a broad spectrum of anti-coronaviral activities [9,10]. In addition, no human protease has high structural homology with the 3CL^{pro} of SARS-CoV-2 [11,12]. Therefore, given the indispensable role of 3CL^{pro} in the viral life cycle [13], the highly conserved structure [14], and the less related homologous protein in humans [15], 3CL^{pro} is an important target for COVID-19 drugs development.

Many covalent peptidomimetics have been reported as 3CL^{pro}

* Corresponding author.
** Corresponding author.
*** Corresponding author.
E-mail addresses: ymzhang@wh.iov.cn (Y. Zhang), suhaixia1@simm.ac.cn (H. Su), qmzhang@simm.ac.cn (Q. Zhang).
[1] These authors contributed equally to this work.

https://doi.org/10.1016/j.ejmech.2023.115512
Received 11 March 2023; Received in revised form 1 May 2023; Accepted 22 May 2023
Available online 23 May 2023

inhibitors against COVID-19 [16–21]. Among the reported covalent 3CL^{pro} inhibitors, Paxlovid (co-packaged of nirmatrelvir tablets and ritonavir tablets) has been approved by the FDA for the treatment of COVID-19 on December 22nd, 2021. The 3CL^{pro} inhibitor nirmatrelvir (Fig. 1) has a potent antiviral effect on the SARS-CoV-2 original strain and variants, but it is easily metabolized by CYP3A4 [22]. Ritonavir, as an inhibitor of CYP3A4, could effectively increase the blood concentration of nirmatrelvir [23]. Because of complex drug-drug interactions, Paxlovid should not be used by many people who are taking other drugs at the same time [24,25]. Therefore, oral peptidomimetic 3CL^{pro} inhibitors with high activity and good pharmacokinetic properties deserve further investigation.

The catalytic pocket of SARS-CoV-2 3CL^{pro} contains cysteine residues (Cys145), which can be covalently bound with electrophilic groups (warheads) [26–29]. In addition to nitriles, the reported warheads of 3CL^{pro} inhibitors were various as shown in Fig. 2, including sulfonates, aldehydes, α-ketoamides, vinyl esters, hydroxymethyl ketones, acyloxymethyl ketones, and benzothiazolyl ketones and so on [16,30–36].

Benzothiazolyl ketone has been reported as a promising covalent warhead bound to Cys145 of 3CL^{pro} [37–39]. Konno. et al. discovered that YH-53, a peptidomimetic benzothiazolyl ketone compound, exhibited conspicuous activity against SARS-CoV-2 3CL^{pro} [40]. Kneller. et al. reported the joint X-ray/neutron structure of the 3CL^{pro}/BBH-1 complex, and the result showed that BBH-1's benzothiazolyl ketone-warhead reacted with Cys145-SH of 3CL^{pro} [41]. Pfizer's researchers reported that a series of compounds with benzothiazolyl ketone as a covalent warhead exhibited various 3CL^{pro} activities and pharmacokinetic properties, such as PF-1. It is worth mentioning that PF-1 and nirmatrelvir showed similar enzyme activity and pharmacokinetic properties [22].

The methyl substituent on the 6, 6-dimethyl-3-azabicyclo [3.1.0] hexane of nirmatrelvir was one of the major metabolic sites [22]. In order to improve pharmacokinetic properties, we carried out structural modifications of metabolic sites, as shown in Fig. 3. First of all, we removed the methyl group of the ternary loop on nirmatrelvir. Due to the instability and high reactivity, the ternary loop was also removed. The NS5A inhibitor ledipasvir formed an [2.2.1] azabicyclic ring instead of a pyrrolidine, which could contribute to improving its pharmacokinetic properties [42]. According to the co-crystal structure of nirmatrelvir with SARS-CoV-2 3CL^{pro} [22], the corresponding cavity in the position of pyrrolidine is large. Inspired by ledipasvir, we adopted the same transformation to convert pyrrolidine into [2.2.1] azabicyclic ring.

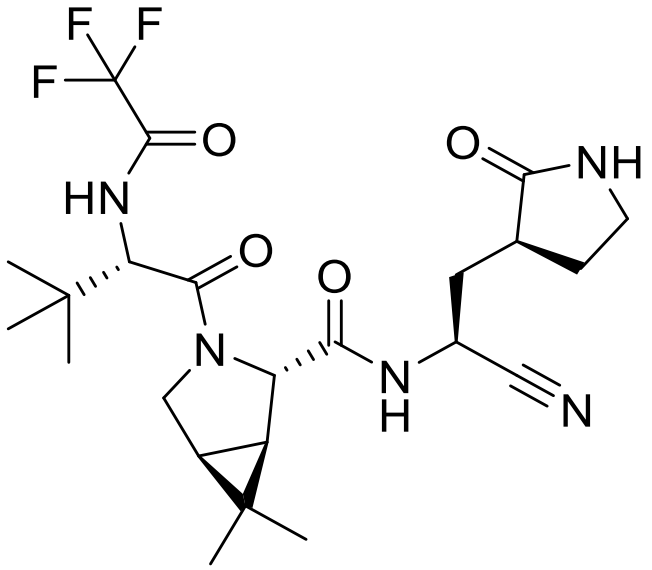

Fig. 1. nirmatrelvir.

In addition, benzothiazolyl ketone was chosen as the warhead.

In order to understand how the compound **A** binds to SARS-CoV-2 3CL^{pro}, molecular docking studies of compound **A** were performed in the active sites of 3CL^{pro} structure (PDB ID:7VH8) using Schrodinger, and the results were summarized in Fig. 4. As shown in Fig. 4A, the binding pattern of compound **A** (light blue) with 3CL^{pro} was similar to that of nirmatrelvir (green), and the [2.2.1] azabicyclic ring of compound **A** could be accommodated well in the binding pocket of the 6, 6-dimethyl-3-azabicyclo [3.1.0] hexane of nirmatrelvir. In the binding model (Fig. 4B), the benzothiazoyl ketone warhead of compound **A** was covalently bound to Cys145, the benzothiazolyl group formed a π-π interaction with His-41, and amide groups interacted with His-164, Glu-166, and Leu-167 to form hydrogen bond interactions.

In summary, we designed and synthesized a series of peptidomimetic compounds containing benzothiazolyl ketone and an [2.2.1] azabicyclic ring in the hope of obtaining 3CL^{pro} inhibitors with high potency and good pharmacokinetic properties.

2. Results and discussion

2.1. Chemistry

The synthesis of the target compounds **11a-11j** was described in Scheme 1. The reaction of commercially available Methyl(*S*)-2-(Boc-amino)-3-[(*S*)-2-oxo-3-pyrrolidinyl]propanoate with *N*, *O*-dimethyl hydroxylamine (HN(OMe)Me·HCl) in the presence of the Grignard reagent i-PrMgCl afforded Weinreb amide **2**. The Weinreb amide **2** was reacted with benzothiazole in the presence of *n*-Butyllithium (*n*-BuLi) via a nucleophilic substitution reaction to give key intermediate **3**. Compound **4** was esterified to obtain the intermediate **5**, which was then deprotected and coupled with different carboxylic acids **6a-6e** to obtain the corresponding *N*-protected amino acid esters **7a-7e**. The intermediates **7a-7e** were deprotected and reacted with trifluoromethanesulfonic anhydride or dimethylsulfamoyl chloride to afford compounds **8a-8e**. Then **8a-8e** were hydrolyzed with lithium hydroxide monohydrate ($LiOH·H_2O$) to furnish the corresponding carboxylic acid fragments **9a-9e**. Using the same conditions, compound **10a** was obtained by hydrolyzing compound **7a**. Compound **3** was deprotected and subsequently coupled with **9a-9e** and **10a** in the presence of the coupling agent *O*-(7-Azabenzotriazol-1-yl)-*N*, *N*, *N*′, *N*′-tetramethyl uronium (HATU) and *N*, *N*-diisopropylethylamine (DIEA) to afford the target compounds **11f-11j** and **11a**. Compound **11a** was deprotected and reacted with different anhydrides and organic acids to obtain the target compounds **11b-11e**.

2.2. Biological activity evaluation

2.2.1. SARS-CoV-2 3CL^{pro} inhibitory activities of compounds *11a-11f*

The crystal structures of 3CL^{pro} with different compounds have been reported [43–45]. As shown in Fig. 4A, the P4 pocket has a polar gap and a hydrophobic cavity. Therefore, acyl and sulfonyl groups connected with different hydrophobic groups are selected at the R_1 position, hoping to obtain compounds with high activity and good pharmacokinetic properties. A series of compounds **11a-11f** were designed, synthesized, and evaluated the inhibitory activities against SARS-CoV-2 3CL^{pro} and nirmatrelvir was used as a positive control. The results were summarized in Table 1. This result showed that compound **11b**, which introduced a trifluoroacetyl group at the R_1 position, displayed the most excellent activity of all the designed compounds (IC_{50} = 0.110 μM), but was lower than that of nirmatrelvir (IC_{50} = 0.035 μM). When the two fluorine atoms of **11b** were replaced with slightly larger methyl groups, the activity of **11c** decreased 11 folds (IC_{50} = 1.268 μM). When replacing the three fluorine atoms of **11b** with the smaller deuterium atoms, the activity of **11d** decreased 5 folds (IC_{50} = 0.527 μM). In addition, the activity of **11a** with the t-butyloxy carbonyl group in the R_1 position decreased 45 times (IC_{50} = 5.003 μM) compared to that of **11b**. The above results indicate that the R_1 position is sensitive to the occupied

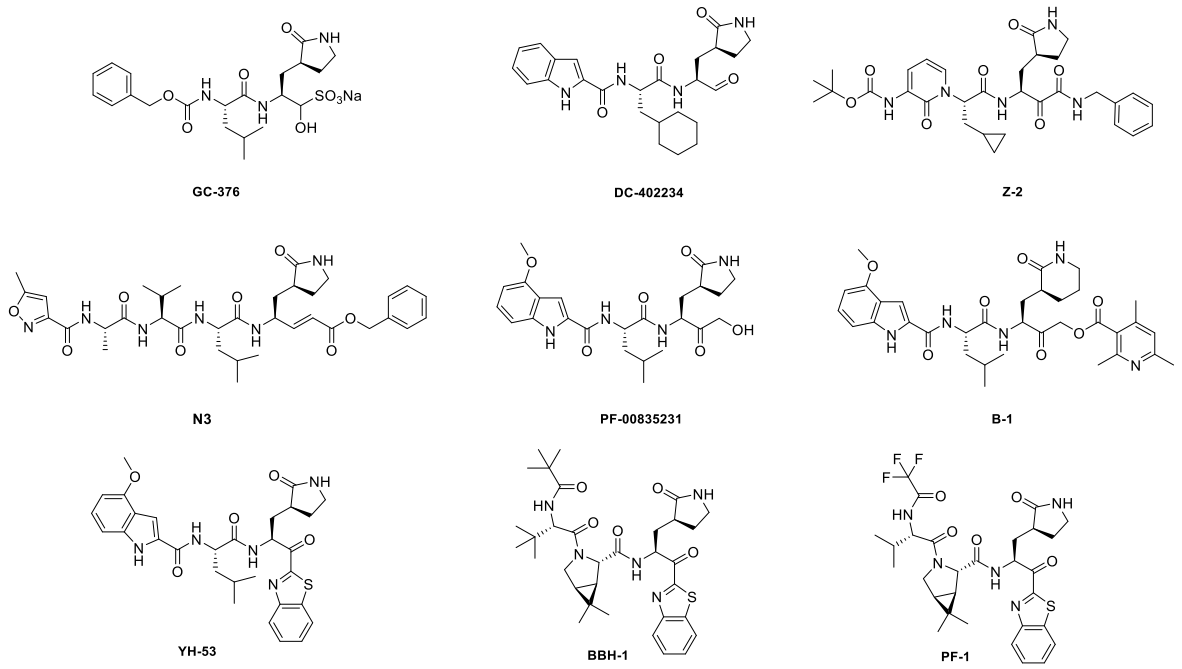

Fig. 2. Structures of some reported peptidomimetic 3CL^{pro} inhibitors.

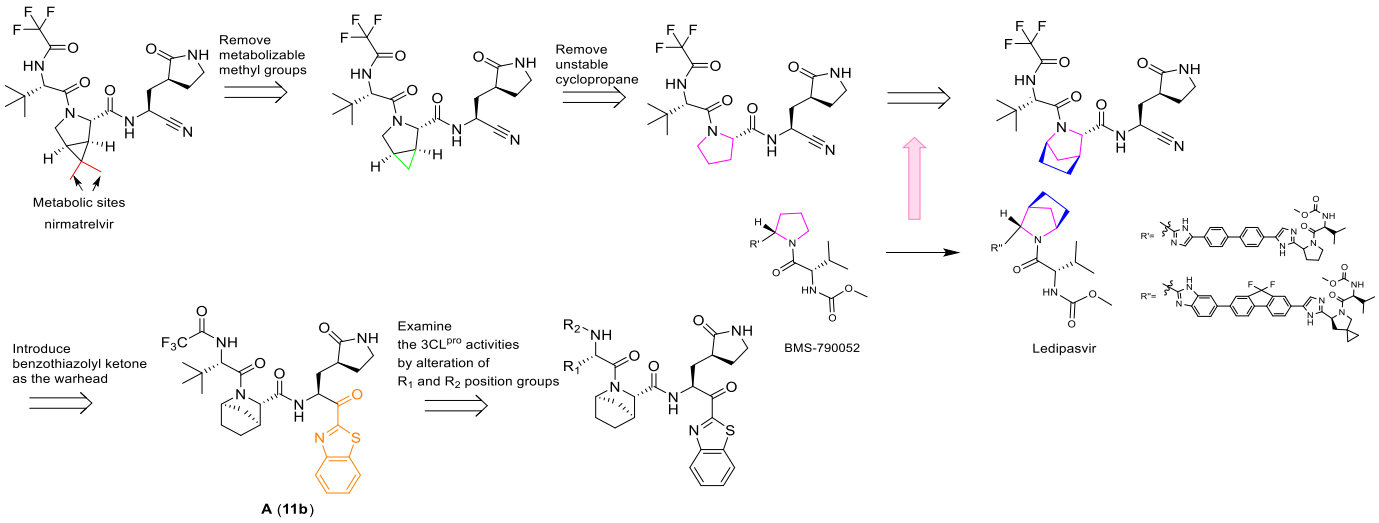

Fig. 3. Design strategy of target compounds.

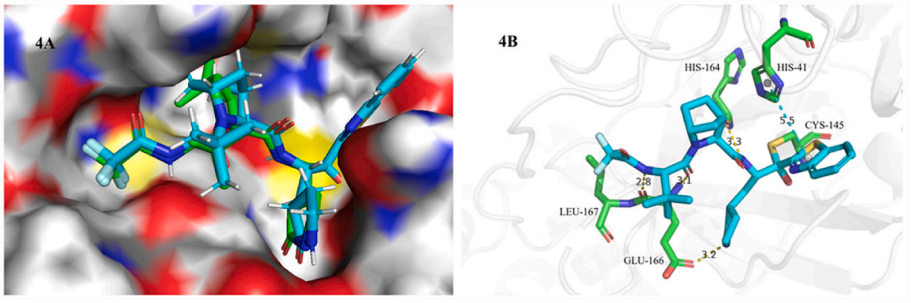

Fig. 4. Binding model of compound **A** into the SARS-CoV-2 3CL^{pro} (PDB ID:7VH8). **4A**. Comparing the binding patterns of compound **A** (blue) and nirmatrelvir (green); **4B**. Interaction of compound **A** (blue) with the residues of SARS-CoV-2 3CL^{pro}, the green dotted lines represented the π-π interaction and the yellow dotted lines represented the hydrogen bond interaction.

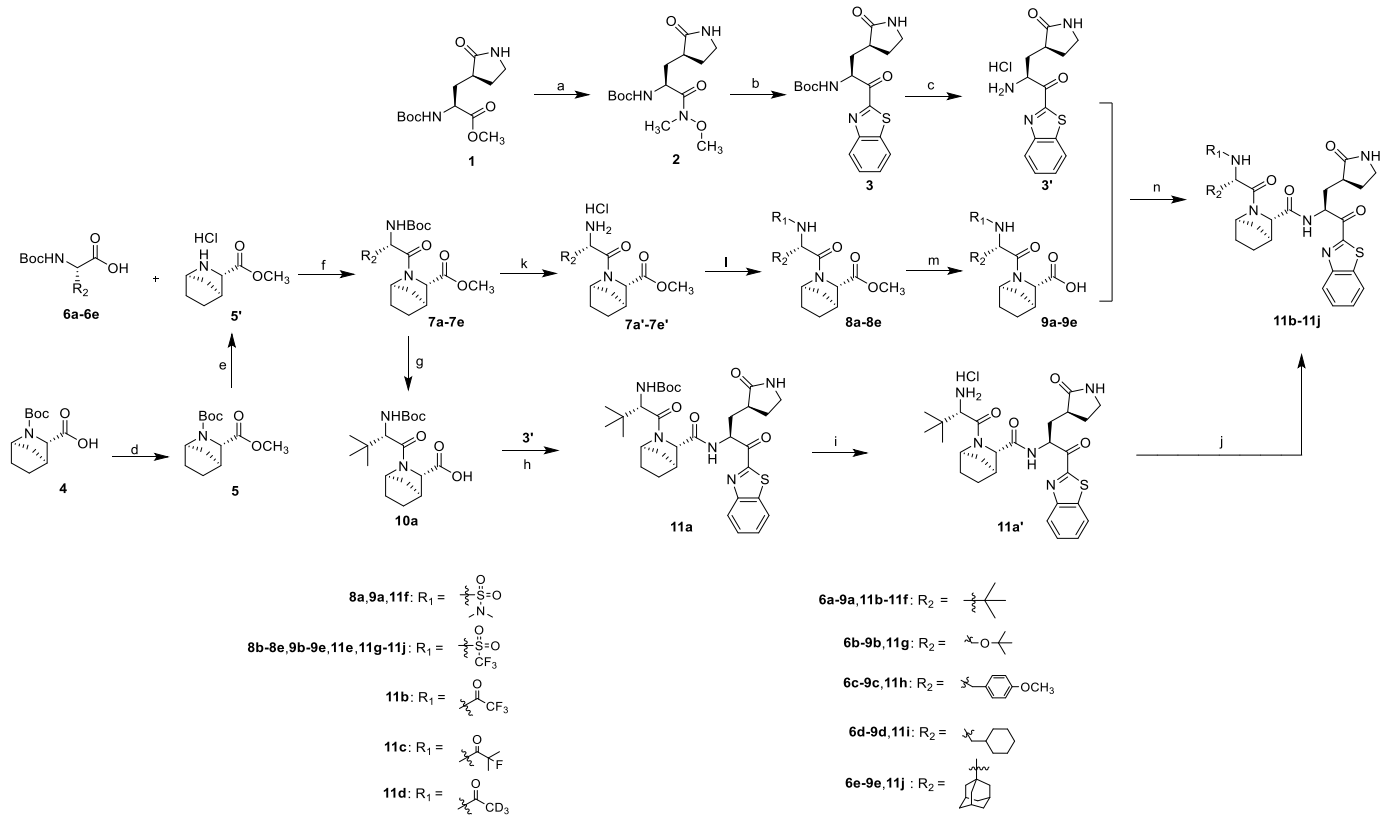

Scheme 1. Synthesis of the target compounds **11a-11j**. Reagents and conditions: (a) HN(OMe)Me·HCl, i-PrMgCl (2 M in THF), THF, 0 °C, 3 h; (b) benzothiazole, *n*-BuLi (1.6 M in THF), THF, −78 °C, 3 h; (c) 4 M HCl in 1, 4-dioxane, DCM, 20–25 °C, 40 min; (d) dimethyl sulfate, NaOH, THF, 65 °C, 2 h; (e) 4 M HCl in 1, 4-dioxane, DCM, 20–25 °C, 40 min; (f) HATU, DIEA, DCM, 20–25 °C, 3–5 h; (g) LiOH·H_2O, THF, H_2O, MeOH, 25 °C, 3 h; (h) HATU, DIEA, DCM/DMF, 20–25 °C, 3–5 h; (i) 4 M HCl in 1, 4-dioxane, DCM, 20–25 °C, 40 min; (j) trifluoroacetic anhydride/2-fluoroisobutyric acid/acetic hydride-d_6/trifluoromethanesulfonic anhydride, Et_3N, DCM, 20–25 °C, overnight; (k) 4 M HCl in 1, 4-dioxane, DCM, 20–25 °C, 40 min; (l) dimethylsulfamoyl chloride/trifluoromethanesulfonic anhydride, Et_3N, DCM, 0 °C, 1 h, and then 25 °C, 1 h; (m) LiOH·H_2O, THF, H_2O, MeOH, 25 °C, 3 h; (n) HATU, DIEA, DCM/DMF, 20–25 °C, 3–5 h.

Table 1
Inhibition activities of compounds **11a-11f** against SARS-CoV-2 $3CL^{pro}$.

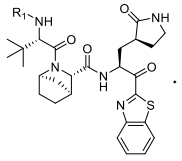

Entry no.	R_1	IC_{50} (μM)
11a		5.003
11b		0.110
11c		1.268
11d		0.527
11e		0.868
11f		0.584
nirmatrelvir[a]		0.035

[a] Used as a positive control.

space of the substituent group. Besides, compound **11e**, which replaced the trifluoroacetyl group of **11b** with a trifluoromethosulfonyl group, showed 8 times lower inhibitory activity against $3CL^{pro}$ (IC_{50} = 0.868 μM) than that of compound **11b**. When replacing the trifluoromethyl group with the dimethylamino group, the activity of compound **11f** (IC_{50} = 0.584 μM) was still lower than that of compound **11b**, although slightly higher than that of compound **11e**.

2.2.2. *Microsomal stability of compounds **11b-11f***

Based on the good enzyme activities and the concern about the metabolic properties of compounds, the microsomal stability tests of compounds **11b-11f** were performed. Nirmatrelvir was used as a positive control. The data on microsomal stability in the species of human and mouse were shown in Table 2. The microsomal stability varied widely between different compounds. Deuteration is a common strategy

Table 2
Microsomal stability of compounds **11b-11f** on species of human and mouse.

Entry no.	$t_{1/2}$ (minute)[b]	
	human	mouse
11b	11.60	7.74
11c	18.03	4.82
11d	42.20	33.75
11e	>120	>120
11f	3.25	0.85
nirmatrelvir[a]	35.5	17.7

[a] Used as a positive control.
[b] The tested concentration of compounds was 1 μM.

to improve metabolic stability in medicinal chemistry. By replacing the trifluoroacetyl group of **11b** with the trideuterium acetyl group, the microsomal stability of **11d** was improved compared with **11b** in both human and mouse species, and was similar to that of nirmatrelvir in human species. The $t_{1/2}$ of **11b** and **11d** were 11.60 min and 42.20 min in the human species, respectively, and 7.74 min and 33.75 min in the mouse species. When the two fluorine atoms of **11b** were replaced with slightly larger methyl groups, the $t_{1/2}$ of **11c** was similar to that of **11b** in both human and mouse species. Compared with other tested compounds, the microsomal stability of compound **11e**, which replaced the trifluoroacetyl group of **11b** with the trifluoromethosulfonyl group, was significantly improved. The $t_{1/2}$ of **11e** in both human and mouse species were more than 120 min. But when replacing the trifluoromethyl group with the dimethylamino group, the $t_{1/2}$ of **11f** decreased significantly compared to compound **11e**.

2.2.3. Pharmacokinetic properties of compounds *11b* and *11e*

Among the tested compounds, **11b** had the best enzymatic potency, and **11e** had the best metabolic stability in *vitro* and good enzyme activity. Therefore, compounds **11b** and **11e** were chosen for further evaluation of their pharmacokinetic properties. The single-dose pharmacokinetics of **11b** and **11e** in ICR mice were given in Table 3. Nirmatrelvir was used as a positive control. This result exhibited that both **11b** and **11e** showed desirable pharmacokinetic properties. Following single-dose oral administration, the $AUC_{(0\text{-}t)}$ of **11e** was 2.4 times higher than that of **11b** and 5 times higher than that of nirmatrelvir. And the C_{max} of **11e** was 2.1 times greater than that of **11b** and 1.8 times greater than that of nirmatrelvir. In addition, the oral bioavailability of compounds **11b** and **11e** was greater than that of nirmatrelvir. And **11e** displayed better oral bioavailability (F = 67.98%) than that of **11b** (F = 47.25%).

2.2.4. SARS-CoV-2 $3CL^{pro}$ inhibitory activities of compounds *11g-11j*

The compound **11e** was chosen for further modification according to its inhibitory activity against $3CL^{pro}$ and pharmacokinetic properties. Because the groups in R_2 position may correspond to a hydrophobic pocket in the structure of $3CL^{pro}$, the hydrophobic groups are preferred at R_2 position. Compounds **11g-11j** were designed, synthesized and evaluated for their inhibitory activities against SARS-CoV-2 $3CL^{pro}$, in which the R_2 position groups were different hydrophobic groups including ethers, p-methoxybenzyl, cyclohexyl methyl and adamantyl. As shown in Table 4, the results showed that the inhibitory activities of these compounds against $3CL^{pro}$ ranged from 1.5 μM to 5.5 μM. When replacing the *tert*-butyl group of **11e** with the tert-butoxymethyl group, the enzyme activity of **11g** decreased 3 times (IC_{50} = 2.741 μM) compared to that of **11e** (IC_{50} = 0.868 μM). By replacing the *tert*-butyl group of **11e** with the p-methoxybenzyl group, the enzyme activity of **11h** decreased 6 times (IC_{50} = 5.335 μM) compared to that of **11e**. When replacing the p-methoxybenzyl group of **11h** with the aliphatic cyclohexyl methyl group, the enzyme activity of **11i** (IC_{50} = 5.140 μM) was slightly decreased compared to **11h**. Among compounds **11g-11j**, compound **11j**, which introduced an adamantyl group at the R_2 position, showed the best enzyme inhibition activity. But the $3CL^{pro}$ inhibitory activity of **11j** (IC_{50} = 1.646 μM) was slightly lower than that of **11e** (IC_{50} = 0.868 μM).

Table 4
Inhibition activities of compounds **11g-11j** against SARS-CoV-2 $3CL^{pro}$.

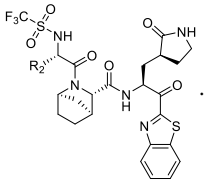

Entry no.	R_2	IC_{50} (μM)
11g		2.741
11h	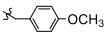	5.335
11i		5.140
11j		1.646
nirmatrelvir [a]		0.035

[a] Used as a positive control.

2.2.5. Pharmacokinetic properties of compound *11j*

Although the enzyme inhibitory activity of **11e,** which replaces the trifluoroacetyl group of **11b** with the trifluoromethosulfonyl group, was slightly lower than that of **11b**, the $AUC_{(0\text{-}t)}$, C_{max} and oral bioavailability of **11e** in ICR mice were significantly improved. Therefore, the pharmacokinetic properties of **11j** whose R_1 position was trifluoromethosulfonyl group, were evaluated. The single-dose pharmacokinetics of **11j** in ICR mice were given in Table 5. The oral bioavailability of **11j** was 48.1%, which was similar to that of **11b** (F = 47.25%). After oral administration, the $AUC_{(0\text{-}t)}$ of **11j** (32473 h*ng/mL) was about 6.3 times higher than that of **11e** (5143 h*ng/mL), and the $T_{1/2}$ of **11j** (2.1 h) was longer than that of **11e** (0.76 h). This result exhibited that compound **11j** showed high plasma exposure after oral administration.

Table 5
Single dose PK of compound **11j**.

Administration[a]	$T_{1/2}$ (h)	C_{max} (ng/mL)	$AUC_{(0\text{-}t)}$ (h*ng/mL)	$AUC_{(0\text{-}\infty)}$ (h*ng/mL)	F (%)
IV	1.38 ± 0.2	-[b]	33780 ± 4258.5	34308 ± 4670	–
PO	2.1 ± 0.8	9327 ± 3316	32473 ± 16572.8	33207 ± 16862	48.1

[a] Single IV dose was 10 mg/kg and PO dose was 20 mg/kg.
[b] Not tested.

Table 3
Single dose PK of compounds **11b** and **11e**.

Entry no.	Administration[a]	$T_{1/2}$ (h)	C_{max} (ng/mL)	$AUC_{(0\text{-}t)}$ (h*ng/mL)	$AUC_{(0\text{-}\infty)}$ (h*ng/mL)	F (%)
11b	IV	0.47 ± 0.09	-[b]	2281 ± 325	2284 ± 324	–
	PO	0.91 ± 0.09	1597 ± 135	2155 ± 168	2161 ± 171	47.25 ± 3.69
11e	IV	0.74 ± 0.04	–	3783 ± 389	3857 ± 388	–
	PO	0.76 ± 0.03	3342 ± 1243	5143 ± 303	5153 ± 306	67.98 ± 4.01
nirmatrelvir[c]	IV	0.42 ± 0.10	–	2240 ± 101	2241 ± 101	–
	PO	0.51 ± 0.10	1819 ± 695	1023 ± 195	1029 ± 202	22.85 ± 4.35

[a] Single IV dose was 10 mg/kg and PO dose was 20 mg/kg.
[b] Not tested.
[c] Used as a positive control.

2.2.6. SARS-CoV-2 antiviral activities and cytotoxicities of 11e and 11j

Finally, the antiviral activity tests against SARS-CoV-2 WIV04 and the cytotoxicity tests in Vero E6 cells of compounds **11e** and **11j** were performed using nirmatrelvir as the positive control. As shown in Table 6, the antiviral activity of compound **11j** (EC_{50} = 0.18 μM) was better than that of nirmatrelvir (EC_{50} = 0.24 μM) and compound **11e** (EC_{50} = 0.32 μM). Besides, the CC_{50} values of **11e** and **11j** were all more than 50 μM. It was worth mentioning that the EC_{50} value (0.18 μM) of the antiviral activity of compound **11j** in Vero E6 cells was lower than the IC_{50} value (1.646 μM) of the $3CL^{pro}$ inhibitory activity. We suspected that the mismatch may be related to many factors, such as the different incubation time of the compound with SARS-CoV-2 $3CL^{pro}$ (10 min) and Vero E6 cells (24 h), and the cell penetration propensity of the compound. The strong hydrophobicity of the benzothiazole unit and the adamantane unit may be conducive to increasing cell penetration [40], but the real reason needs to be deeply explored in the future.

In summary, in addition to high plasma exposure after oral administration in ICR mice, **11j** exhibited excellent anti-SARS-CoV-2 activity in Vero E6 cells and a large security window (SI = 300). Besides, the C_{max} of **11j** was 70 times greater than its EC_{50} in Vero E6 cells. The mouse plasma concentrations at different time after oral administration of 20 mg/kg **11j** and the ratio of plasma concentration to EC_{50} were shown in Table S1.

2.2.7. Protease inhibition selectivity of compound 11j

To evaluate the protease inhibition selectivity of **11j** between $3CL^{pro}$ and the other cysteine proteases, the inhibitory activities of **11j** against chymotrypsin, cathepsin B and cathepsin L were tested. As shown in Table 7, the inhibition of **11j** against chymotrypsin, cathepsin B and cathepsin L at 20 μM was 55.79%, −32.93% and 26.96%, respectively. Based on the inhibitory activity of **11j** against SARS-CoV-2 $3CL^{pro}$ (IC_{50} = 1.646 μM), **11j** displayed high inhibition selectivity between $3CL^{pro}$ and other tested cysteine proteases.

3. Conclusion

In an effort to develop high efficiency, low toxicity, and oral peptidomimetic $3CL^{pro}$ inhibitors, a series of peptidomimetic compounds were designed, synthesized, and evaluated. The SARS-CoV-2 $3CL^{pro}$ inhibition activities of compounds **11a-11f**, in which the substituent of R_1 included different acyl and sulfonyl groups, were evaluated. The compounds displayed varied enzyme inhibition activities and the structure-activity relationship (SAR) of **11a-11f** were discussed. The microsomal stability tests showed the half-life of **11e** in both species of human and mouse were more than 120 min. Next, compound **11e** showed a high $AUC_{(0\text{-}t)}$ (po, 20 mg/kg, 5143 h*ng/mL) and better oral bioavailability (F = 67.98%) in ICR mice. The compounds **11g-11j**, in which the R_2 position groups were different hydrophobic groups, were derivatives of **11e**. Among them, the $AUC_{(0\text{-}t)}$ of **11j** (po, 20 mg/kg, 32473 h*ng/mL) was 6.3 times greater than that of **11e** (po, 20 mg/kg, 5143 h*ng/mL) in ICR mice. Furthermore, both compounds **11e** and **11j** showed good antiviral activities and low cytotoxicities (CC_{50} > 50 μM) in Vero E6 cells. The EC_{50} value of **11e** was 0.32 μM and the EC_{50} value of **11j** was 0.18 μM. Besides, **11j** displayed high inhibition selectivity between $3CL^{pro}$ and other tested cysteine proteases. In summary, **11j** was recognized as a promising lead compound in the development of oral $3CL^{pro}$ inhibitors for the treatment of a more comprehensive population of COVID-19.

Table 6
Antiviral activities against SARS-CoV-2 WIV04 and cytotoxicities in Vero E6 cells of compounds **11e** and **11j**.

Entry no.	EC_{50} (μM)	CC_{50} (μM)	SI[a]
11e	0.32	137.4	429
11j	0.18	53.99	300
nirmatrelvir[b]	0.24	>500	>2083

[a] SI = CC_{50}/EC_{50}.
[b] Used as a positive control.

Table 7
Protease inhibition by compound **11j**.

Protease	Inhibition (%)[a], 20 μM
Chymotrypsin	55.79
Cathepsin B	−32.93
Cathepsin L	26.96

[a] Data presented is the mean value of two independent determinations.

4. Experimental section

4.1. Materials and methods

Reagents and solvents were commercial and were used without further purification. ^1H NMR and ^{13}C NMR spectra were recorded using a Bruker 400 MHz, 500 MHz, 600 MHz, or 800 MHz spectrometer with tetramethylsilane as an internal standard. High-resolution mass spectra (HRMS) were measured on a Micromass Ultra Q-TOF spectrometer. All target compounds possessed a purity of ≥95% as determined by HPLC. HPLC analysis was performed using an Agilent 1260 instrument or a Thermo Scientific UltiMate 3000 instrument. The HPLC methods for the target compounds were shown in Table S2.

4.2. Synthesis of 3 and 5

4.2.1. Synthetic procedure for the preparation of tert-butyl((S)-1-(benzo[d]thiazol-2-yl) -3-((S)-2-oxopyrrolidin-3-yl)propan-2-yl) carbamate (3)

In a 500 mL round bottom flask, starting materials Methyl (*S*)-2-(Boc-amino)-3-[(*S*)-2-oxo-3-pyrrolidinyl] propanoate (8 g, 28 mmol) and *N*, *O*-dimethylhydroxylamine hydrochloride (6.817 g, 70 mmol) were added, followed by the addition of dry THF (80 mL) under nitrogen protection. And the solution was added dropwise to isopropyl magnesium chloride (i-PrMgCl) (98 mL, 2 M in THF) over 30 min using a constant pressure drip funnel at 0 °C, and the solution was stirred for 3 h. The reaction was quenched with a saturated ammonium chloride solution. The mixture was extracted with ethyl acetate, and then dried over Na_2SO_4. The organic layer was concentrated under reduced pressure, and the resulting residue was purified by eluting through a silica gel column with a 2:1 PE/acetone solvent system to give the pure compound **2** (8.2 g). Yield 90% from **1**; white solid; ^1H NMR (500 MHz, DMSO-d_6): δ 7.62 (s, 1H), 7.00 (dd, *J* = 179.1, 7.0 Hz, 1H), 4.39 (dd, *J* = 34.4, 26.8 Hz, 1H), 3.72 (s, 3H), 3.34–3.33 (m, 1H), 3.17–3.12 (m, 2H), 3.10 (s, 3H), 2.34–2.22 (m, 1H), 2.19–2.12 (m, 1H), 1.94–1.84 (m, 1H), 1.66–1.57 (m, 1H), 1.36 (s, 9H). ^{13}C NMR (126 MHz, DMSO-d_6): δ 178.13, 155.60, 77.99, 61.18, 49.15, 39.44, 37.74, 32.36, 28.20, 27.26. ESI-MS: *m/z* 316.4 $[M + H]^+$.

To a solution of benzothiazole (6.9 mL, 63.49 mmol) in THF (40 mL) at −78 °C was added *n*-BuLi (1.6 M in THF, 28 mL) dropwise over 30 min under nitrogen protection. After 1 h of stirring, the Weinreb amide **2** (4 g, 12.7 mmol) in THF (25 mL) was slowly added over 15 min, and the solution was stirred for 3 h. The reaction was quenched with a saturated ammonium chloride solution. The mixture was extracted with ethyl acetate, and then dried over Na_2SO_4. The organic layer was concentrated under reduced pressure, and the resulting residue was purified by eluting through a silica gel column with a 3:1 PE/acetone solvent system to give the pure compound **3** (3.9 g). Yield 79% from **2**; yellow solid; ^1H NMR (400 MHz, DMSO-d_6): δ 8.25 (t, *J* = 8.6 Hz, 2H), 7.74 (d, *J* = 7.0 Hz, 1H), 7.70–7.61 (m, 3H), 5.27 (s, 1H), 3.23–3.16 (m, 2H), 2.27 (s, 1H), 2.07–1.99 (m, 1H), 1.83 (dt, *J* = 21.5, 10.8 Hz, 2H), 1.45–1.26 (m, 9H). ^{13}C NMR (101 MHz, DMSO-d_6): δ 193.75, 178.09, 164.49, 155.66, 152.92, 136.31, 128.14, 127.50, 125.18, 123.17, 78.40, 54.95, 38.08,

31.89, 28.11, 27.37. ESI-MS: *m/z* 390.2 $[M + H]^+$.

4.2.2. Synthesis of 2-(tert-butyl) 3-methyl (1R,3S,4S)-2-azabicyclo[2.2.1] heptane-2,3- dicarboxylate (5)

To a solution of (*3S*)-*N*-Boc-2-azabicyclo [2.2.1] heptane-3-carboxylic acid (10 g, 41.45 mmol) in THF (150 mL) at 60 °C was added an aqueous sodium hydroxide solution (2.5 g, 62.17 mmol) and dimethyl sulfate (6 mL, 62.17 mmol) respectively and slowly at the same time. Then the solution was stirred for 2 h. The reaction was monitored by TLC. To the cooled reaction was added 100 mL of water, and the mixture was extracted with ethyl acetate, and then dried over Na_2SO_4. The organic layer was concentrated under reduced pressure, and the resulting residue was purified by eluting through a silica gel column with a 10:1 PE/EA solvent system to give the pure compound **5** (9 g). Yield 87% from **4**; colorless oil; ^{1}H NMR (400 MHz, DMSO-d_6): δ 4.12 (d, J = 29.4 Hz, 1H), 3.71 (d, J = 6.2 Hz, 1H), 3.63 (d, J = 7.7 Hz, 3H), 2.59 (s, 1H), 1.71 (dd, J = 24.9, 9.9 Hz, 2H), 1.64–1.56 (m, 1H), 1.49 (d, J = 6.3 Hz, 2H), 1.35 (d, J = 33.5 Hz, 9H), 1.28–1.23 (m, 1H). ^{13}C NMR (126 MHz, DMSO-d_6): δ 171.10, 170.89, 153.22, 152.02, 78.79, 78.60, 63.57, 63.44, 56.92, 55.54, 51.68, 41.99, 41.37, 34.71, 34.05, 30.09, 29.87, 28.06, 27.85, 27.15, 27.06. ESI-MS: *m/z* 256.0 $[M + H]^+$.

4.3. Synthesis of 7a-7e

The carboxylic acids **6a-6e** were commercially available.

4.3.1. Synthesis of methyl (1R,3S,4S)-2-((S)-2-((tert-butoxycarbonyl) amino) -3,3- dimethylbutanoyl)-2-azabicyclo[2.2.1]heptane-3-carboxylate (7a)

To a solution of the *N*-Boc protected amine **5** (4 g, 15.69 mmol) in DCM (30 mL) was added 4 M HCl in 1, 4-dioxane (40 mL, 156.9 mmol) under nitrogen protection at 20–25 °C. After stirring for 40 min, the mixture was concentrated under reduced pressure to obtain the intermediate **3'**. Then, to a solution of **3'** in DCM (40 mL), *N-tert*-Butylcarbamoyl-*L*-tert-leucine **6a** (3.628 g, 15.69 mmol), and HATU (6.259 g, 15.69 mmol) were added. The resulting solution was cooled to 0 °C under ice bath conditions, and DIEA (8.2 mL, 47.07 mmol) was then added dropwise under nitrogen protection. After adding, the ice bath was removed and the mixture was allowed to stir for 3–5 h at 20–25 °C. Then, the solvent was evaporated under reduced pressure, and the residue was dissolved in ethyl acetate. The organic layer was washed with a saturated ammonium chloride solution and brine. This solution was dried over Na_2SO_4, filtered, and evaporated under reduced pressure to give the compound **7a** (5.2 g) without further purification. Yield 90% from **5**; faint yellow solid; ^{1}H NMR (400 MHz, DMSO-d_6): δ 6.42 (d, J = 9.2 Hz, 1H), 4.55 (s, 1H), 4.21 (d, J = 9.4 Hz, 1H), 3.86 (s, 1H), 3.60 (s, 3H), 2.61 (s, 1H), 1.81 (d, J = 9.8 Hz, 1H), 1.66 (t, J = 11.2 Hz, 4H), 1.48 (dd, J = 18.4, 13.6 Hz, 2H), 1.37 (s, 9H), 0.95 (s, 9H). ^{13}C NMR (126 MHz, DMSO-d_6): δ 170.29, 168.41, 155.46, 78.14, 63.21, 58.33, 58.08, 51.71, 40.71, 35.12, 34.66, 30.78, 28.17, 27.11, 26.21. ESI-MS: *m/z* 369.3 $[M + H]^+$.

The compounds **7b-7e** were prepared from **6b-6e** with **5**, using a method similar to that described for the synthesis of **7a**.

4.3.2. methyl(1R,3S,4S)-2-(N-(tert-butoxycarbonyl)-O-(tert-butyl)-L-seryl)-2-azabi cyclo[2.2.1]heptane-3-carboxylate (7b)

Yield 88% from **5**; white solid; ^{1}H NMR (500 MHz, DMSO-d_6): δ 6.84 (d, J = 8.3 Hz, 1H), 4.48 (s, 1H), 4.28 (dd, J = 14.2, 6.9 Hz, 1H), 3.80 (s, 1H), 3.59 (s, 3H), 3.42–3.36 (m, 2H), 2.60 (s, 1H), 1.88 (d, J = 9.2 Hz, 1H), 1.69 (d, J = 13.6 Hz, 4H), 1.45 (s, 1H), 1.36 (s, 9H), 1.13 (s, 9H). ^{13}C NMR (126 MHz, DMSO-d_6): δ 170.13, 167.91, 155.08, 78.11, 72.67, 63.28, 61.95, 57.31, 52.33, 51.64, 42.42, 40.72, 38.25, 35.08, 33.30, 30.43, 28.19, 28.09, 27.11, 27.03. ESI-MS: *m/z* 421.5 $[M + Na]^+$.

4.3.3. methyl(1R,3S,4S)-2-((S)-2-((tert-butoxycarbonyl)amino)-3-(4-methoxyphenyl) propanoyl) -2-azabicyclo[2.2.1]heptane-3-carboxylate (7c)

Yield 87% from **5**; white solid; ^{1}H NMR (500 MHz, DMSO-d_6): δ 7.23 (d, J = 8.5 Hz, 2H), 7.03 (d, J = 8.5 Hz, 1H), 6.83 (d, J = 8.6 Hz, 2H), 4.28 (td, J = 8.8, 5.6 Hz, 1H), 4.18 (s, 1H), 3.82 (s, 1H), 3.71 (s, 3H), 3.62 (s, 3H), 2.81 (dd, J = 13.9, 5.5 Hz, 1H), 2.71 (dd, J = 14.6, 9.6 Hz, 1H), 2.59 (s, 1H), 1.77 (d, J = 9.7 Hz, 1H), 1.70–1.61 (m, 3H), 1.43 (dd, J = 12.5, 7.0 Hz, 1H), 1.33 (s, 1H), 1.30 (s, 9H). ^{13}C NMR (126 MHz, DMSO-d_6): δ 170.26, 169.04, 157.85, 155.14, 130.43, 129.57, 113.46, 77.97, 63.25, 57.31, 54.99, 53.60, 51.74, 40.63, 36.37, 35.18, 30.51, 28.16, 27.08. ESI-MS: *m/z* 455.4 $[M + Na]^+$.

4.3.4. methyl(1R,3S,4S)-2-((S)-2-((tert-butoxycarbonyl)amino)-3-cyclohexylpropanoyl) -2- azabicyclo[2.2.1]heptane-3-carboxylate (7d)

Yield 89% from **5**; yellow solid; ^{1}H NMR (500 MHz, DMSO-d_6): δ 6.99 (d, J = 8.5 Hz, 1H), 4.28–4.19 (m, 2H), 3.81 (s, 1H), 3.59 (s, 3H), 2.69 (s, 2H), 2.60 (s, 1H), 1.81 (dd, J = 18.2, 11.5 Hz, 2H), 1.69–1.60 (m, 6H), 1.46 (dd, J = 18.0, 8.1 Hz, 2H), 1.36 (s, 9H), 1.32 (s, 1H), 1.18 (ddd, J = 28.1, 12.2, 6.9 Hz, 4H), 0.95–0.84 (m, 2H). ^{13}C NMR (126 MHz, DMSO-d_6): δ 170.28, 169.80, 155.39, 77.90, 62.98, 57.26, 51.73, 49.23, 40.65, 38.86, 38.25, 35.12, 33.43, 33.39, 31.88, 30.74, 28.22, 27.05, 26.06, 25.98, 25.78. ESI-MS: *m/z* 409.3 $[M + H]^+$.

4.3.5. methyl(1R,3S,4S)-2-((S)-2-((3S,5S,7S)-adamantan-1-yl)-2-((tert-butoxycarbonyl) amino) acetyl)-2-azabicyclo[2.2.1]heptane-3-carboxylate (7e)

Yield 92% from **5**; white solid; ^{1}H NMR (500 MHz, DMSO-d_6): δ 6.32 (d, J = 9.2 Hz, 1H), 4.54 (s, 1H), 4.07 (d, J = 9.4 Hz, 1H), 3.87 (s, 1H), 3.61 (s, 3H), 2.61 (s, 1H), 1.92 (s, 4H), 1.80 (d, J = 9.6 Hz, 1H), 1.66 (d, J = 18.2 Hz, 12H), 1.58 (d, J = 11.6 Hz, 4H), 1.37 (s, 9H). ^{13}C NMR (126 MHz, DMSO-d_6): δ 170.22, 167.79, 155.46, 78.08, 63.25, 59.14, 58.33, 51.71, 40.68, 37.51, 36.42, 36.25, 35.18, 30.73, 28.15, 27.78, 27.08. ESI-MS: *m/z* 447.4 $[M + H]^+$.

4.4. Synthesis of methyl(1R,3S,4S)-2-((S)-2-((N,N-dimethylsulfamoyl) amino)-3,3- dimethylbutanoyl)-2-azabicyclo[2.2.1]heptane-3-carboxylate (8a)

To a solution of the compound **7a** (368 mg, 1 mmol) in DCM (2 mL) was added 4 M HCl in 1, 4-dioxane (2.5 mL, 10 mmol) under nitrogen protection at 20–25 °C. After stirring for 40 min, the mixture was concentrated under reduced pressure to obtain the intermediate **7a'**. Then, to a solution of **7a'** and DCM (2 mL), DIEA (0.52 mL, 3 mmol) was added dropwise, along with dimethylsulfamoyl chloride (93 μL, 0.9 mmol) at 0 °C under nitrogen protection. After adding, the mixture was allowed to stir at 0 °C for 1 h. Then, the ice bath was removed, and the solution was allowed to stir for 1 h at 25 °C. The organic layer was washed with a 1 M HCl solution and brine. This solution was dried over Na_2SO_4, filtered and evaporated under reduced pressure. The resulting residue was purified by eluting through a silica gel column with a 200:1 DCM/MeOH solvent system to give the pure compound **8a** (300 mg). Yield 80% from **7a**; white solid; ^{1}H NMR (400 MHz, DMSO-d_6): δ 7.12 (d, J = 10.1 Hz, 1H), 4.53 (s, 1H), 3.85 (s, 1H), 3.76 (d, J = 10.1 Hz, 1H), 3.62 (s, 3H), 2.63 (s, 1H), 2.58 (s, 6H), 1.82 (d, J = 9.8 Hz, 1H), 1.75–1.63 (m, 3H), 1.46 (t, J = 9.9 Hz, 1H), 1.38 (d, J = 9.7 Hz, 1H), 1.00 (s, 9H). ^{13}C NMR (126 MHz, DMSO-d_6): δ 170.24, 167.60, 63.47, 61.10, 58.16, 51.68, 40.59, 37.62, 35.17, 35.08, 29.70, 27.24, 26.31. ESI-MS: *m/z* 376.4 $[M + H]^+$.

4.5. Synthesis of 8b-8e

4.5.1. Synthesis of methyl (1R,3S,4S)-2-(O-(tert-butyl)-N-((trifluoromethyl)sulfonyl) -L-seryl)-2-azabicyclo[2.2.1]heptane-3-carboxylate (8b)

To a solution of the compound **7b** (1 g, 2.42 mmol) in DCM (5 mL)

was added 4 M HCl in 1, 4-dioxane (6.1 mL, 24.2 mmol) under nitrogen protection at 20–25 °C. After 40 min of stirring, the mixture was concentrated under reduced pressure. Then, to a solution of the corresponding deprotected mixture and DCM (15 mL), Et_3N (1 mL, 7.25 mmol) was added dropwise, and trifluoromethanesulfonic anhydride (406 μL, 2.42 mmol) at 0 °C under nitrogen protection. After adding, the mixture was allowed to stir for 1 h at 0 °C. Then, the ice bath was removed, and the solution was allowed to stir for 1 h at 25 °C. The organic layer was washed with a 1 M HCl solution and brine. This solution was dried over Na_2SO_4, filtered, and evaporated under reduced pressure. The resulting residue was purified by eluting through a silica gel column with a 150:1 DCM/MeOH solvent system to give the pure compound **8b** (530 mg). Yield 51% from **7b**; white solid; ^{1}H NMR (500 MHz, DMSO-d_6): δ 10.10 (d, J = 8.6 Hz, 1H), 4.44 (s, 1H), 4.21 (dd, J = 8.9, 4.4 Hz, 1H), 3.88 (s, 1H), 3.61 (d, J = 3.3 Hz, 3H), 3.50–3.43 (m, 2H), 2.64 (d, J = 1.7 Hz, 1H), 1.88 (d, J = 9.9 Hz, 1H), 1.75–1.68 (m, 2H), 1.54–1.46 (m, 2H), 1.40 (d, J = 9.9 Hz, 1H), 1.16 (d, J = 3.2 Hz, 9H). ^{13}C NMR (126 MHz, DMSO-d_6): δ 169.76, 165.89, 73.29, 63.46, 61.95, 57.62, 56.14, 51.78, 40.62, 35.14, 30.32, 26.95. ESI-MS: m/z 431.2 $[M + H]^+$.

The compounds **8c-8e** were prepared from **7c-7e** with trifluoromethanesulfonic anhydride using a method similar to that described for the synthesis of **8b.**

*4.5.2. Synthesis of methyl (1R,3S,4S)-2-((S)-3-(4-methoxyphenyl)-2-((trifluoromethyl) sulfonamido)propanoyl)-2-azabicyclo [2.2.1] heptane-3-carboxylate (**8c**)*

Yield 52% from **7c**; white solid; ^{1}H NMR (500 MHz, DMSO-d_6): δ 10.03 (d, J = 8.6 Hz, 1H), 7.23 (d, J = 8.6 Hz, 2H), 6.80 (d, J = 8.6 Hz, 2H), 4.13 (s, 1H), 4.09 (td, J = 9.1, 5.1 Hz, 1H), 3.83 (s, 1H), 3.66 (s, 3H), 3.57 (s, 3H), 2.88 (dd, J = 14.0, 5.0 Hz, 1H), 2.68 (dd, J = 14.0, 9.7 Hz, 1H), 2.56 (s, 1H), 1.70 (d, J = 9.9 Hz, 1H), 1.66–1.58 (m, 2H), 1.44–1.36 (m, 2H), 1.28 (d, J = 9.8 Hz, 1H). ^{13}C NMR (126 MHz, DMSO-d_6): δ 169.86, 167.33, 158.25, 130.72, 127.82, 113.63, 63.40, 57.90, 57.56, 55.03, 51.87, 40.52, 37.26, 35.29, 30.45, 26.90. ESI-MS: m/z 463.2 $[M - H]^-$.

*4.5.3. Synthesis of methyl(1R,3S,4S)-2-((S)-3-cyclohexyl-2-((trifluoromethyl) sulfonamido)propanoyl)-2-azabicyclo [2.2.1] heptane-3-carboxylate (**8d**)*

Yield 54% from **7d**; white solid; ^{1}H NMR (500 MHz, DMSO-d_6): δ 9.96 (d, J = 8.4 Hz, 1H), 4.19–4.12 (m, 2H), 3.89 (s, 1H), 3.61 (s, 3H), 2.65 (s, 1H), 1.83 (t, J = 11.4 Hz, 2H), 1.74–1.68 (m, 4H), 1.65–1.59 (m, 2H), 1.57–1.40 (m, 6H), 1.18 (dt, J = 18.0, 5.6 Hz, 3H), 1.02–0.92 (m, 2H). ^{13}C NMR (126 MHz, DMSO-d_6): δ 169.88, 167.98, 63.13, 57.42, 53.46, 51.85, 40.48, 35.17, 33.21, 33.05, 31.19, 30.55, 26.87, 25.90, 25.58. ESI-MS: m/z 441.5 $[M + H]^+$.

4.5.4. Synthesis of methyl (1R,3S,4S)-2-((S)-2-((3S,5S,7S)-adamantan-1-yl)-2-((trifluoromethyl)sulfonamido)acetyl)-2-azabicyclo [2.2.1] heptane-3-carboxylate (8e)

Yield 50% from **7e**; white solid; ^{1}H NMR (500 MHz, DMSO-d_6): δ 9.50 (d, J = 9.3 Hz, 1H), 4.58 (s, 1H), 3.92 (d, J = 9.3 Hz, 1H), 3.87 (s, 1H), 3.63 (s, 3H), 2.63 (d, J = 2.9 Hz, 1H), 1.96 (s, 3H), 1.80 (d, J = 9.9 Hz, 1H), 1.72 (dd, J = 19.1, 8.2 Hz, 4H), 1.69–1.64 (m, 6H), 1.56 (dd, J = 23.4, 11.9 Hz, 5H), 1.45 (t, J = 9.4 Hz, 1H), 1.38 (d, J = 9.8 Hz, 1H). ^{13}C NMR (126 MHz, DMSO-d_6): δ 170.03, 165.40, 63.70, 58.38, 51.80, 40.57, 37.27, 36.78, 36.13, 35.25, 29.89, 27.74, 27.08. ESI-MS: m/z 479.5 $[M + H]^+$.

4.6. Synthesis of 9a-9e, 10a

*4.6.1. Synthesis of (1R, 3S, 4S)-2-((S)-2-((N, N-dimethylsulfamoyl) amino)-3,3-dimethylbutanoyl)-2-azabicyclo [2.2.1] heptane-3-carboxylic acid (**9a**)*

To a solution of the compound **8a** (300 mg, 0.8 mmol) in THF (2 mL) at room temperature, added $LiOH{\cdot}H_2O$ (50 mg, 1.2 mmol) in water (1 mL) and methanol (1 mL). After stirring for 3 h at 25 °C, the solvent was evaporated under reduced pressure, and the resulting residue was dissolved in water. The pH of the mixture was adjusted to 3–4 by adding 1 M HCl (aq) dropwise. Then, the precipitated white solid was filtered and dried to obtain the compound **9a** (270 mg). Yield 93% from **8a**; white solid; ^{1}H NMR (500 MHz, DMSO-d_6): δ 12.45 (s, 1H), 7.12 (d, J = 10.1 Hz, 1H), 4.48 (s, 1H), 3.74 (d, J = 11.4 Hz, 2H), 2.61 (d, J = 2.7 Hz, 1H), 2.57 (s, 6H), 1.85 (d, J = 9.7 Hz, 1H), 1.68 (ddd, J = 30.3, 19.4, 6.5 Hz, 3H), 1.42 (dd, J = 13.7, 6.7 Hz, 1H), 1.35 (d, J = 9.6 Hz, 1H), 0.99 (s, 9H). ^{13}C NMR (126 MHz, DMSO-d_6): δ 171.20, 167.51, 63.81, 61.13, 58.16, 40.57, 37.61, 35.12, 35.08, 29.77, 27.41, 26.35. ESI-MS: m/z 362.4 $[M + H]^+$.

The compounds 9b-9e and 10a were prepared from 8b-8e and 7a, using a method similar to that described for the synthesis of 9a.

4.6.2. Synthesis of (1R, 3S, 4S)-2-(O-(tert-butyl)-N-((trifluoromethyl) sulfonyl)-L-seryl)-2-azabicyclo [2.2.1] heptane-3-carboxylic acid (9b)

Yield 96% from **8b**; white solid; ^{1}H NMR (500 MHz, DMSO-d_6): δ 12.49 (s, 1H), 10.09 (s, 1H), 4.39 (s, 1H), 4.20 (t, J = 6.7 Hz, 1H), 3.78 (s, 1H), 3.51–3.48 (m, 1H), 3.43 (d, J = 6.3 Hz, 1H), 2.64 (s, 1H), 1.90 (d, J = 9.8 Hz, 1H), 1.71 (t, J = 8.2 Hz, 2H), 1.48 (dd, J = 29.3, 9.0 Hz, 2H), 1.38 (d, J = 9.7 Hz, 1H), 1.15 (s, 9H). ^{13}C NMR (126 MHz, DMSO-d_6): δ 170.65, 165.81, 73.26, 63.82, 61.95, 57.61, 56.40, 40.57, 35.07, 30.43, 26.97. ESI-MS: m/z 417.3 $[M + H]^+$.

*4.6.3. Synthesis of (1R, 3S, 4S)-2-((S)-3-(4-methoxyphenyl)-2-((trifluoromethyl) sulfonamido)propanoyl)-2-azabicyclo [2.2.1] heptane-3-carboxylic acid (**9c**)*

Yield 92% from **8c**; white solid; ^{1}H NMR (500 MHz, DMSO-d_6): δ 12.59 (s, 1H), 10.09 (s, 1H), 7.30 (d, J = 8.5 Hz, 2H), 6.86 (d, J = 8.6 Hz, 2H), 4.23 (s, 1H), 4.14 (d, J = 5.1 Hz, 1H), 3.81 (s, 1H), 3.73 (s, 3H), 2.96 (dd, J = 14.1, 4.6 Hz, 1H), 2.75 (dd, J = 14.0, 10.0 Hz, 1H), 2.64 (s, 1H), 1.83 (d, J = 9.8 Hz, 1H), 1.74–1.67 (m, 2H), 1.50 (t, J = 9.3 Hz, 1H), 1.43 (t, J = 9.1 Hz, 1H), 1.36 (d, J = 9.7 Hz, 1H). ^{13}C NMR (126 MHz, DMSO-d_6): δ 170.76, 167.33, 158.21, 130.72, 113.63, 63.75, 58.08, 57.57, 55.03, 40.50, 37.29, 35.24, 30.57, 27.09. ESI-MS: m/z 451.3 $[M + H]^+$.

*4.6.4. Synthesis of (1R, 3S, 4S)-2-((S)-3-cyclohexyl-2-((trifluoromethyl) sulfonamido) propanoyl)-2-azabicyclo [2.2.1] heptane-3-carboxylic acid (**9d**)*

Yield 93% from **8d**; white solid; ^{1}H NMR (800 MHz, DMSO-d_6): δ 12.53 (s, 1H), 9.94 (d, J = 8.1 Hz, 1H), 4.15 - 4.12 (m, 2H), 3.79 (s, 1H), 2.64 (s, 1H), 1.86 (d, J = 10.0 Hz, 1H), 1.81 (d, J = 12.2 Hz, 1H), 1.70 (ddd, J = 14.0, 9.7, 6.0 Hz, 4H), 1.64–1.60 (m, 2H), 1.58–1.55 (m, 1H), 1.50 (d, J = 11.0 Hz, 1H), 1.48–1.45 (m, 1H), 1.44–1.41 (m, 2H), 1.39 (d, J = 9.9 Hz, 1H), 1.21 (ddd, J = 12.1, 7.6, 2.6 Hz, 1H), 1.17–1.13 (m, 2H), 0.98 (ddd, J = 26.1, 17.2, 7.3 Hz, 2H). ^{13}C NMR (201 MHz, DMSO-d_6): δ 170.77, 167.92, 63.51, 57.38, 53.52, 40.46, 35.10, 33.24, 33.05, 31.19, 30.60, 27.05, 25.91, 25.58. ESI-MS: m/z 427.5 $[M + H]^+$.

*4.6.5. Synthesis of (1R, 3S, 4S)-2-((S)-2-((3S, 5S, 7S)-adamantan-1-yl)-2-((trifluoro methyl)sulfonamido)acetyl)-2-azabicyclo [2.2.1] heptane-3-carboxylic acid (**9e**)*

Yield 96% from **8e**; white solid; ^{1}H NMR (500 MHz, DMSO-d_6): δ 12.50 (s, 1H), 9.49 (d, J = 9.3 Hz, 1H), 4.54 (s, 1H), 3.91 (d, J = 9.3 Hz, 1H), 3.77 (s, 1H), 2.62 (d, J = 3.5 Hz, 1H), 1.94 (s, 3H), 1.86 (d, J = 9.8 Hz, 1H), 1.80–1.70 (m, 4H), 1.65 (dd, J = 17.7, 12.2 Hz, 6H), 1.55 (dd, J = 25.6, 11.6 Hz, 5H), 1.42 (t, J = 10.4 Hz, 1H), 1.36 (d, J = 9.6 Hz, 1H). ^{13}C NMR (126 MHz, DMSO-d_6): δ 171.11, 165.26, 63.75, 58.32, 40.47, 37.23, 36.81, 36.11, 35.11, 29.99, 27.78, 27.26. ESI-MS: m/z 465.4 $[M + H]^+$.

4.6.6. Synthesis of (1R, 3S, 4S)-2-((S)-2-((tert-butoxycarbonyl)amino)-3,3-dimethyl butanoyl)-2-azabicyclo [2.2.1] heptane-3-carboxylic acid (10a)

Yield 96% from **7a**; white solid; ^{1}H NMR (400 MHz, DMSO-d_6): δ 12.39 (s, 1H), 6.36 (d, J = 9.3 Hz, 1H), 4.52 (s, 1H), 4.20 (d, J = 9.5 Hz, 1H), 3.77 (s, 1H), 2.60 (s, 1H), 1.85 (d, J = 11.4 Hz, 1H), 1.78–1.50 (m, 4H), 1.45–1.41 (m, 1H), 1.37 (s, 9H), 0.95 (s, 9H). ^{13}C NMR (126 MHz, DMSO-d_6): δ 171.20, 168.30, 155.40, 78.08, 63.53, 58.30, 58.05, 40.66, 35.02, 34.71, 30.85, 28.14, 27.26, 26.22. ESI-MS: m/z 355.3 $[M + H]^+$.

4.7. Synthesis of 11a-11j

4.7.1. Synthesis of tert-butyl ((S)-1-((1R,3S,4S)-3-(((S)-1-(benzo[d]thiazol-2-yl)-1-oxo -3-((S)-2-oxopyrrolidin-3-yl)propan-2-yl)carbamoyl)-2-azabicyclo[2.2.1]heptan-2-yl)-3,3-dimethyl-1-oxobutan-2-yl)carbamate (11a)

To a solution of the intermediate **3** (660 mg, 1.69 mmol) in DCM (4 mL) was added 4 M HCl in 1, 4-dioxane (4.3 mL, 16.9 mmol) under nitrogen protection at 20–25 °C. After stirring for 40 min, the mixture was concentrated under reduced pressure to obtain the intermediate **3'**. Then, to a solution of **3'** in DCM (5 mL) and DMF (5 mL), the compound **10a** (600 mg, 1.69 mmol), and HATU (677 mg, 1.69 mmol) were added. The resulting solution was cooled to 0 °C under ice bath conditions, and DIEA (884 μL, 5.07 mmol) was then added dropwise under nitrogen protection. After adding, the ice bath was removed and the mixture was allowed to stir for 3–5 h at 20–25 °C. Then, the dichloromethane was evaporated under reduced pressure, and the residue was dissolved in ethyl acetate. The organic layer was washed with a saturated ammonium chloride solution and brine. This solution was dried over Na_2SO_4, filtered, and evaporated under reduced pressure. The resulting crude compound was purified by silica gel column chromatography using 200:1 DCM/MeOH as eluents to obtain compound **11a** (602 mg). Yield 57% from **10a**; white solid; ^{1}H NMR (500 MHz, DMSO-d_6): δ 8.67 (d, J = 7.9 Hz, 1H), 8.27 (dd, J = 7.2, 1.8 Hz, 1H), 8.24–8.21 (m, 1H), 7.66 (td, J = 7.0, 1.4 Hz, 2H), 7.63 (s, 1H), 6.47 (d, J = 9.2 Hz, 1H), 5.59 (ddd, J = 11.4, 8.1, 3.0 Hz, 1H), 4.48 (d, J = 10.3 Hz, 1H), 4.18 (d, J = 9.3 Hz, 1H), 3.91 (s, 1H), 3.19 (t, J = 9.1 Hz, 1H), 3.10 (dd, J = 16.5, 9.1 Hz, 1H), 2.58 (td, J = 11.3, 3.5 Hz, 1H), 2.46 (s, 1H), 2.33–2.26 (m, 1H), 2.09–2.03 (m, 1H), 1.98 (d, J = 9.4 Hz, 1H), 1.82–1.76 (m, 2H), 1.65 (s, 3H), 1.37 (s, 9H), 1.28–1.19 (m, 2H), 0.94 (s, 9H). ^{13}C NMR (126 MHz, DMSO-d_6): δ 193.15, 178.15, 169.95, 168.04, 164.31, 155.51, 152.90, 136.38, 128.19, 127.56, 125.18, 123.22, 77.97, 64.04, 58.19, 58.09, 52.80, 41.16, 37.58, 34.83, 34.54, 32.83, 30.87, 28.16, 27.48, 27.35, 26.30. ESI-MS: m/z 626.3 $[M + H]^+$. HRMS (ESI): m/z calcd for $C_{32}H_{44}N_5O_6S$ $[M + H]^+$ 626.3007, found 626.3007. HPLC purity: 95.15% (Rt: 17.464 min).

The compounds **11f-11j** were prepared from **9a-9e** with **3**, using a method similar to that described for the synthesis of **11a**.

4.7.2. Synthesis of (1R, 3S, 4S)-N-((S)-1-(benzo[d]thiazol-2-yl)-1-oxo-3-((S)-2-oxo pyrrolidin-3-yl)propan-2-yl)-2-((S)-2-((N,N-dimethylsulfamoyl)amino)-3,3-dimethyl butanoyl)-2-azabicyclo [2.2.1] heptane-3-carboxamide (11f)

Yield 57% from **9a**; white solid; ^{1}H NMR (500 MHz, DMSO-d_6): δ 8.69 (d, J = 8.2 Hz, 1H), 8.29–8.26 (m, 1H), 8.24–8.20 (m, 1H), 7.67 (dq, J = 6.9, 5.6 Hz, 2H), 7.63 (s, 1H), 7.12 (d, J = 10.0 Hz, 1H), 5.64 (ddd, J = 11.5, 8.3, 3.0 Hz, 1H), 4.44 (s, 1H), 3.93 (s, 1H), 3.75 (d, J = 10.0 Hz, 1H), 3.20–3.09 (m, 2H), 2.59 (s, 6H), 2.48 (s, 1H), 2.34–2.28 (m, 1H), 2.08–1.99 (m, 2H), 1.85–1.76 (m, 2H), 1.72–1.60 (m, 3H), 1.33 (d, J = 10.8 Hz, 1H), 1.23 (s, 2H), 0.98 (s, 9H). ^{13}C NMR (126 MHz, DMSO-d_6): δ 193.11, 178.22, 169.87, 167.30, 164.29, 152.91, 136.39, 128.22, 127.58, 125.19, 123.24, 64.22, 61.14, 58.04, 52.64, 41.13, 37.64, 37.57, 35.13, 34.84, 32.99, 29.93, 27.47, 26.37. ESI-MS: m/z 633.4 $[M + H]^+$. HRMS (ESI): m/z calcd for $C_{29}H_{41}N_6O_6S_2$ $[M + H]^+$ 633.2524, found 633.2529. HPLC purity: 96.96% (Rt: 7.952 min).

4.7.3. Synthesis of (1R, 3S, 4S)-N-((S)-1-(benzo[d]thiazol-2-yl)-1-oxo-3-((S)-2-oxo pyrrolidin-3-yl)propan-2-yl)-2-(O-(tert-butyl)-N-((trifluoromethyl)sulfonyl)-L-seryl)-2-azabicyclo [2.2.1] heptane-3-carboxamide (11g)

Yield 43% from **9b**; white solid; ^{1}H NMR (800 MHz, DMSO-d_6): δ 10.11 (s, 1H), 8.64 (s, 1H), 8.27 (d, J = 8.0 Hz, 1H), 8.21 (d, J = 7.9 Hz, 1H), 7.67–7.65 (m, 3H), 5.42 (t, J = 7.6 Hz, 1H), 4.33 (s, 1H), 4.20 (s, 1H), 3.90 (s, 1H), 3.59–3.56 (m, 1H), 3.41 (d, J = 8.0 Hz, 1H), 3.20 (d, J = 8.9 Hz, 1H), 3.13 (d, J = 7.3 Hz, 1H), 2.47 (dd, J = 10.5, 3.6 Hz, 1H), 2.43 (s, 1H), 2.30–2.27 (m, 1H), 2.09 (d, J = 10.3 Hz, 1H), 2.05 (d, J = 8.9 Hz, 1H), 1.81 (ddd, J = 12.6, 9.2, 5.4 Hz, 2H), 1.68 (d, J = 7.7 Hz, 2H), 1.53 (s, 1H), 1.36–1.33 (m, 1H), 1.22 (d, J = 4.1 Hz, 1H), 1.15 (s, 9H). ^{13}C NMR (201 MHz, DMSO-d_6): δ 193.26, 178.65, 169.78, 164.90, 153.32, 136.78, 128.61, 128.01, 125.53, 123.68, 73.80, 65.17, 58.14, 53.70, 41.47, 38.13, 35.49, 32.82, 30.98, 27.76, 27.56, 27.49, 27.35. ^{19}F NMR (753 MHz, DMSO-d_6): δ −77.33. ESI-MS: m/z 688.3 $[M + H]^+$. HRMS (ESI): m/z calcd for $C_{29}H_{37}F_3N_5O_7S_2$ $[M + H]^+$ 688.2081, found 688.20. HPLC purity: 95.02% (Rt: 17.845 min).

4.7.4. Synthesis of (1R, 3S, 4S)-N-((S)-1-(benzo[d]thiazol-2-yl)-1-oxo-3-((S)-2-oxo pyrrolidin-3-yl)propan-2-yl)-2-((S)-3-(4-methoxyphenyl)-2-((trifluoromethyl)sulfonamido)propanoyl)-2-azabicyclo [2.2.1] heptane-3-carboxamide (11h)

Yield 45% from **9c**; white solid; ^{1}H NMR (500 MHz, DMSO-d_6): δ 10.11 (d, J = 8.7 Hz, 1H), 8.74 (d, J = 7.3 Hz, 1H), 8.28 (d, J = 5.2 Hz, 1H), 8.23 (dd, J = 7.2, 1.7 Hz, 1H), 7.69–7.65 (m, 3H), 7.30 (d, J = 8.6 Hz, 2H), 6.86 (d, J = 8.6 Hz, 2H), 5.45–5.42 (m, 1H), 4.24 (s, 1H), 4.12 (dd, J = 9.6, 3.6 Hz, 1H), 3.92 (s, 1H), 3.72 (s, 3H), 3.22–3.18 (m, 1H), 3.11 (d, J = 10.2 Hz, 1H), 2.73–2.68 (m, 1H), 2.45 (s, 1H), 2.32 (dd, J = 11.8, 5.9 Hz, 1H), 2.11 (d, J = 11.0 Hz, 1H), 2.02–1.99 (m, 1H), 1.86–1.80 (m, 2H), 1.69 (s, 2H), 1.51 (d, J = 10.5 Hz, 1H), 1.35 (d, J = 11.7 Hz, 1H), 1.28 (d, J = 9.5 Hz, 1H), 1.23 (d, J = 5.0 Hz, 2H). ^{13}C NMR (201 MHz, DMSO-d_6): δ 192.85, 178.18, 169.45, 167.82, 164.46, 158.16, 152.86, 136.32, 130.64, 128.21, 128.15, 127.54, 125.10, 123.22, 113.63, 64.68, 58.21, 57.58, 55.00, 53.39, 40.94, 37.79, 37.14, 35.20, 32.25, 30.59, 27.34, 27.13. ESI-MS: m/z 722.4 $[M + H]^+$. HRMS (ESI): m/z calcd for $C_{32}H_{35}F_3N_5O_7S_2$ $[M + H]^+$ 722.1925, found 722.1922. HPLC purity: 96.44% (Rt: 17.868 min).

4.7.5. Synthesis of (1R, 3S, 4S)-N-((S)-1-(benzo[d]thiazol-2-yl)-1-oxo-3-((S)-2-oxo pyrrolidin-3-yl)propan-2-yl)-2-((S)-3-cyclohexyl-2-((trifluoromethyl)sulfonamido)propanoyl)-2-azabicyclo [2.2.1] heptane-3-carboxamide (11i)

Yield 48% from **9d**; white solid; ^{1}H NMR (500 MHz, DMSO-d_6): δ 9.98 (d, J = 8.5 Hz, 1H), 8.73 (d, J = 7.3 Hz, 1H), 8.27 (d, J = 1.7 Hz, 1H), 8.23–8.21 (m, 1H), 7.66 (dd, J = 11.1, 4.4 Hz, 3H), 5.41–5.37 (m, 1H), 4.13 (d, J = 8.2 Hz, 1H), 4.10 (s, 1H), 3.89 (s, 1H), 3.20 (d, J = 8.7 Hz, 1H), 3.14 (d, J = 7.2 Hz, 1H), 2.65 (dd, J = 18.2, 16.3 Hz, 1H), 2.44 (s, 1H), 2.40–2.28 (m, 1H), 2.30–2.24 (m, 1H), 2.12–2.06 (m, 1H), 1.98 (s, 1H), 1.83–1.77 (m, 3H), 1.69 (d, J = 6.3 Hz, 3H), 1.59–1.49 (m, 4H), 1.34–1.28 (m, 2H), 1.23 (d, J = 5.0 Hz, 2H), 1.14 (dd, J = 22.9, 11.2 Hz, 3H), 0.95 (dd, J = 19.9, 10.3 Hz, 2H). ^{13}C NMR (126 MHz, DMSO-d_6): δ 192.87, 178.10, 169.46, 168.30, 164.44, 152.86, 136.31, 128.15, 127.54, 125.09, 123.22, 64.32, 57.35, 53.58, 53.35, 40.92, 37.72, 35.03, 33.25, 33.03, 32.19, 31.14, 30.62, 27.27, 27.09, 25.94, 25.84, 25.54. ^{19}F NMR (753 MHz, DMSO-d_6): δ −77.69. ESI-MS: m/z 698.5 $[M + H]^+$. HRMS (ESI): m/z calcd for $C_{31}H_{39}F_3N_5O_6S_2$ $[M + H]^+$ 698.2288, found 698.2296. HPLC purity: 95.47% (Rt: 3.570 min).

4.7.6. Synthesis of (S)-1-(benzo[d]thiazol-2-yl)-1-oxo-3-((S)-2-oxopyrrolidin-3-yl)pro pan-2-yl(1R,3S,4S)-2-((S)-2-((3S,5S,7S)-adamantan-1-yl)-2-((trifluoromethyl)sulfonamido)acetyl)-2-azabicyclo [2.2.1]heptane-3-carboxylate (11j)

Yield 47% from **9e**; white solid; ^{1}H NMR (500 MHz, DMSO-d_6): δ 9.65 (d, J = 9.3 Hz, 1H), 8.69 (d, J = 9.1 Hz, 1H), 8.28 (dd, J = 7.0, 2.1 Hz, 1H), 8.22 (dd, J = 7.1, 2.0 Hz, 1H), 7.70–7.65 (m, 2H), 7.62 (s, 1H),

5.74 (ddd, J = 11.9, 9.2, 2.5 Hz, 1H), 4.53 (s, 1H), 3.92 (d, J = 7.8 Hz, 2H), 3.18 (d, J = 9.1 Hz, 1H), 3.03 (d, J = 7.4 Hz, 1H), 2.60 (d, J = 10.6 Hz, 1H), 2.43 (s, 1H), 2.40–2.35 (m, 1H), 2.11 (d, J = 9.2 Hz, 1H), 2.02 (d, J = 12.1 Hz, 1H), 1.94 (s, 3H), 1.79 (t, J = 14.7 Hz, 5H), 1.69–1.62 (m, 8H), 1.59 (d, J = 11.8 Hz, 3H), 1.49 (d, J = 11.2 Hz, 1H), 1.31–1.25 (m, 2H). ^{13}C NMR (126 MHz, DMSO-d_6): δ 192.89, 178.41, 169.64, 164.81, 164.32, 152.93, 136.40, 128.22, 127.60, 125.16, 123.25, 64.29, 63.67, 58.17, 52.18, 40.99, 37.36, 37.18, 36.82, 36.16, 34.86, 33.60, 30.09, 27.86, 27.38. ^{19}F NMR (471 MHz, DMSO-d_6): δ −77.08. ESI-MS: m/z 736.4 $[M + H]^+$. HRMS (ESI): m/z calcd for $C_{34}H_{41}F_3N_5O_6S_2$ $[M + H]^+$ 736.2445, found 736.2447. HPLC purity: 97.20% (Rt: 3.887 min).

4.8. Synthesis of **11b**-**11e**

4.8.1. Synthesis of (1R,3S,4S)-N-((S)-1-(benzo[d]thiazol-2-yl)-1-oxo-3-((S)-2-oxopyrr olidin-3-yl)propan-2-yl)-2-((S)-3,3-dimethyl-2-(2,2,2-trifluoroacetamido)butanoyl)-2- azabicyclo[2.2.1]heptane-3-carboxamide (11b)

To a solution of the compound **11a** (300 mg, 0.48 mmol) in DCM (1 mL) was added 4 M HCl in 1, 4-dioxane (1.2 mL, 4.8 mmol) under nitrogen protection at 20–25 °C. After stirring for 40 min, the mixture was concentrated under reduced pressure to obtain the intermediate **11a'**. Then, to a solution of **11a'** and DCM (5 mL), Et_3N (2 mL, 1.44 mmol) and trifluoroacetic anhydride (67 μL, 0.48 mmol) were added dropwise at 0 °C under nitrogen protection. After adding, the ice bath was removed and the solution was allowed to stir all night at 20–25 °C. The organic layer was washed with a 1 M HCl solution and brine. This solution was dried over Na_2SO_4, filtered, and evaporated under reduced pressure. The resulting residue was purified by eluting through a silica gel column with a 150:1 DCM/MeOH solvent system to give the pure compound **11b** (100 mg). Yield 32% from **11a**; white solid; ^{1}H NMR (500 MHz, DMSO-d_6): δ 8.67 (d, J = 7.9 Hz, 1H), 8.27 (dd, J = 7.2, 1.8 Hz, 1H), 8.24–8.21 (m, 1H), 7.66 (td, J = 7.0, 1.4 Hz, 2H), 7.63 (s, 1H), 6.47 (d, J = 9.2 Hz, 1H), 5.59 (ddd, J = 11.4, 8.1, 3.0 Hz, 1H), 4.48 (d, J = 10.3 Hz, 1H), 4.18 (d, J = 9.3 Hz, 1H), 3.91 (s, 1H), 3.19 (t, J = 9.1 Hz, 1H), 3.10 (dd, J = 16.5, 9.1 Hz, 1H), 2.58 (td, J = 11.3, 3.5 Hz, 1H), 2.46 (s, 1H), 2.33–2.26 (m, 1H), 2.09–2.03 (m, 1H), 1.98 (d, J = 9.4 Hz, 1H), 1.82–1.76 (m, 2H), 1.65 (s, 3H), 1.37 (s, 9H), 1.28–1.19 (m, 2H), 0.94 (s, 9H). ^{13}C NMR (126 MHz, DMSO-d_6): δ 193.15, 178.15, 169.95, 168.04, 164.31, 155.51, 152.90, 136.38, 128.19, 127.56, 125.18, 123.22, 77.97, 64.04, 58.19, 58.09, 52.80, 41.16, 37.58, 34.83, 34.54, 32.83, 30.87, 28.16, 27.48, 27.35, 26.30. ESI-MS: m/z 626.3 $[M + H]^+$. HRMS (ESI): m/z calcd for $C_{32}H_{44}N_5O_6S$ $[M + H]^+$ 626.3007, found 626.3007. HPLC purity: 95.15% (Rt: 9.760 min).

4.8.2. Synthesis of (1R,3S,4S)-N-((S)-1-(benzo[d]thiazol-2-yl)-1-oxo-3-((S)-2-oxopy rrolidin-3-yl)propan-2-yl)-2-((S)-2-(2-fluoro-2-methylpropanamido)-3,3-dimethylbutanoyl)-2-azabicyclo[2.2.1]heptane-3-carboxamide (11c)

To a solution of the compound **11a** (300 mg, 0.48 mmol) in DCM (4 mL) was added 4 M HCl in 1, 4-dioxane (1.2 mL, 4.8 mmol) under nitrogen protection at 20–25 °C. After stirring for 40 min, the mixture was concentrated under reduced pressure to obtain the intermediate **11a'**. Then, to a solution of **11a'** and DCM (5 mL), the 2-fluoroisobutyric acid (46 μL, 0.48 mmol), and HATU (192 mg, 0.48 mmol) were added. The resulting solution was cooled to 0 °C under ice bath conditions, and DIEA (250 μL, 1.44 mmol) was then added dropwise under nitrogen protection. After adding, the ice bath was removed, and the mixture was allowed to stir all night at 20–25 °C. Then, the dichloromethane was evaporated under reduced pressure, and the residue was dissolved in ethyl acetate. The organic layer was washed with a saturated ammonium chloride solution and brine. This solution was dried over Na_2SO_4, filtered, and evaporated under reduced pressure. The resulting crude compound was purified by silica gel column chromatography using 200:1 DCM/MeOH as eluents to obtain the compound **11c** (170 mg). Yield 58% from **11a**; white solid; ^{1}H NMR (800 MHz, DMSO-d_6): δ 8.71 (d, J = 7.7 Hz, 1H), 8.27 (t, J = 5.9 Hz, 1H), 8.23 (d, J = 7.8 Hz, 1H), 7.68–7.64 (m, 3H), 7.06 (dd, J = 17.8, 13.2 Hz, 1H), 5.59–5.56 (m, 1H), 4.53 (d, J = 9.1 Hz, 2H), 3.94 (s, 1H), 3.20 (t, J = 9.2 Hz, 1H), 3.11 (d, J = 9.0 Hz, 1H), 2.56–2.52 (m, 1H), 2.32–2.28 (m, 1H), 2.07 (dd, J = 26.9, 13.1 Hz, 1H), 1.96 (d, J = 9.0 Hz, 1H), 1.81 (dd, J = 21.4, 10.5 Hz, 2H), 1.65 (dd, J = 28.0, 11.9 Hz, 3H), 1.52–1.49 (m, 3H), 1.45 (d, J = 22.2 Hz, 3H), 1.39–1.37 (m, 1H), 1.27–1.18 (m, 2H), 0.94 (d, J = 24.6 Hz, 9H). ^{13}C NMR (201 MHz, DMSO-d_6): δ 193.10, 178.07, 171.48, 171.37, 169.73, 167.01, 164.27, 152.90, 136.38, 128.20, 127.56, 125.19, 123.22, 96.26, 95.37, 64.09, 58.15, 55.80, 54.91, 52.95, 41.19, 37.65, 35.37, 34.74, 32.71, 30.98, 27.41, 27.25, 26.07, 25.29, 25.17, 24.47, 24.35. ^{19}F NMR (753 MHz, DMSO-d_6): δ −145.33. ESI-MS: m/z 614.4 $[M + H]^+$. HRMS (ESI): m/z calcd for $C_{31}H_{41}FN_5O_5S$ $[M + H]^+$ 614.2807, found 614.281. HPLC purity: 97.42% (Rt: 12.635 min).

4.8.3. Synthesis of (1R, 3S, 4S)-2-((S)-2-(acetamido-2,2,2-d3)-3,3-dimethylbutanoyl) -N-((S)-1-(benzo[d]thiazol-2-yl)-1-oxo-3-((S)-2-oxopyrrolidin-3-yl)propan-2-yl)-2- azabicyclo [2.2.1] heptane-3-carboxamide (11d)

To a solution of the compound **11a** (300 mg, 0.48 mmol) in DCM (1 mL) was added 4 M HCl in 1, 4-dioxane (1.2 mL, 4.8 mmol) under nitrogen protection at 20–25 °C. After 40 min of stirring, the mixture was concentrated under reduced pressure. Then, to a solution of the corresponding deprotected mixture and DCM (5 mL), Et_3N (2 mL, 1.44 mmol) and acetic anhydride-d_6 (46 μL, 0.48 mmol) were added dropwise at 0 °C under nitrogen protection. After adding, the ice bath was removed and the solution was allowed to stir all night at 20–25 °C. The organic layer was washed with a 1 M HCl solution and brine. This solution was dried over Na_2SO_4, filtered, and evaporated under reduced pressure. The resulting residue was purified by eluting through a silica gel column with a 150:1 DCM/MeOH solvent system to give the pure compound **11d** (150 mg). Yield 55% from **11a**; yellow solid; ^{1}H NMR (500 MHz, DMSO-d_6): δ 8.66 (d, J = 8.2 Hz, 1H), 8.27 (dd, J = 7.2, 1.8 Hz, 1H), 8.22 (dd, J = 7.2, 1.6 Hz, 1H), 7.86 (d, J = 9.2 Hz, 1H), 7.66 (td, J = 7.1, 1.4 Hz, 2H), 7.63 (s, 1H), 5.63 (ddd, J = 11.6, 8.3, 3.1 Hz, 1H), 4.54 (d, J = 9.2 Hz, 1H), 4.48 (s, 1H), 3.89 (s, 1H), 3.19 (t, J = 9.1 Hz, 1H), 3.12–3.06 (m, 1H), 2.59 (dt, J = 11.5, 5.8 Hz, 1H), 2.45 (s, 1H), 2.34–2.28 (m, 1H), 2.08–1.99 (m, 2H), 1.83–1.76 (m, 2H), 1.61 (d, J = 11.9 Hz, 3H), 1.34 (d, J = 9.5 Hz, 1H), 1.24 (d, J = 9.4 Hz, 1H), 0.96 (s, 9H). ^{13}C NMR (126 MHz, DMSO-d_6): δ 193.15, 178.26, 169.92, 169.15, 167.73, 164.32, 152.91, 136.40, 128.20, 127.57, 125.18, 123.23, 64.09, 58.12, 56.24, 52.63, 41.12, 37.53, 34.89, 34.57, 33.01, 30.80, 27.47, 27.31, 26.38. ESI-MS: m/z 571.4 $[M + H]^+$. HRMS (ESI): m/z calcd for $C_{29}H_{35}D_3N_5O_5S$ $[M + H]^+$ 571.2776, found 571.2779. HPLC purity: 95.72% (Rt: 9.556 min).

4.8.4. Synthesis of (1R, 3S, 4S)-N-((S)-1-(benzo[d]thiazol-2-yl)-1-oxo-3-((S)-2-oxopy rrolidin-3-yl)propan-2-yl)-2-((S)-3,3-dimethyl-2-((trifluoromethyl)sulfonamido)butanoyl)-2-azabicyclo [2.2.1] heptane-3-carboxamide (11e)

To a solution of the compound **11a** (300 mg, 0.48 mmol) in DCM (1 mL) was added 4 M HCl in 1, 4-dioxane (1.2 mL, 4.8 mmol) under nitrogen protection at 20–25 °C. After stirring for 40 min, the mixture was concentrated under reduced pressure. Then, to a solution of the corresponding deprotected mixture **11a'** and DCM (5 mL), Et_3N (2 mL, 1.44 mmol) was added dropwise, along with trifluoromethanesulfonic anhydride (81 μL, 0.48 mmol) at 0 °C under nitrogen protection. After adding, the ice bath was removed, and the solution was allowed to stir all night at 20–25 °C. The organic layer was washed with a 1 M HCl solution and brine. This solution was dried over Na_2SO_4, filtered, and evaporated under reduced pressure. The resulting residue was purified by eluting through a silica gel column with a 150:1 DCM/MeOH solvent system to give the pure compound **11e** (100 mg). Yield 32% from **11a**; white solid; ^{1}H NMR (500 MHz, DMSO-d_6): δ 9.63 (d, J = 9.4 Hz, 1H), 8.72 (d, J = 8.6 Hz, 1H), 8.28 (dd, J = 7.0, 2.1 Hz, 1H), 8.22 (dd, J = 7.2, 2.0 Hz, 1H), 7.70–7.65 (m, 2H), 7.64 (s, 1H), 5.68 (ddd, J = 11.7, 8.6,

2.8 Hz, 1H), 4.54 (s, 1H), 4.07 (d, $J = 9.5$ Hz, 1H), 3.94 (s, 1H), 3.18 (d, $J = 9.1$ Hz, 1H), 3.11–3.06 (m, 1H), 2.60 (dt, $J = 18.6$, 5.8 Hz, 1H), 2.46 (s, 1H), 2.32 (dd, $J = 12.7$, 7.1 Hz, 1H), 2.02 (dd, $J = 9.3$, 4.4 Hz, 2H), 1.81 (dt, $J = 22.3$, 10.7 Hz, 2H), 1.70–1.61 (m, 2H), 1.52 (t, $J = 9.3$ Hz, 1H), 1.33 (d, $J = 6.0$ Hz, 1H), 1.24 (d, $J = 7.5$ Hz, 1H), 1.03 (s, 9H). ^{13}C NMR (126 MHz, DMSO-d_6): δ 193.02, 178.25, 169.65, 165.57, 164.27, 152.91, 136.41, 128.24, 127.60, 125.19, 123.25, 64.18, 62.76, 58.16, 52.49, 41.10, 37.48, 35.41, 34.79, 33.19, 30.10, 27.45, 27.36, 26.15. ESI-MS: *m/z* 658.4 $[M + H]^+$. HRMS (ESI): *m/z* calcd for $C_{28}H_{35}F_3N_5O_6S_2$ $[M + H]^+$ 658.1975, found 658.1979. HPLC purity: 96.47% (Rt: 4.101 min).

4.9. Molecular docking procedure

The X-ray structure of SARS-CoV-2 3CL^{pro} (PDB ID: 7VH8) was downloaded from the RCSB protein data bank. The molecular docking was performed using the Glide Covalent Docking module in the software package Schrödinger Suite 2020 to perform protein-ligand interaction studies.

4.10. Biological experimental methods

4.10.1. SARS-CoV-2 3CL^{pro} inhibition assay for **11a-11j**

A fluorescence resonance energy transfer (FRET) protease assay was applied to measure the inhibitory activity of compounds against SARS-CoV-2 3CL^{pro}. The recombinant SARS-CoV-2 3CL^{pro} at a concentration of 40 nM was mixed with serial dilutions of each compound in 80 μL of assay buffer (50 mM Tris-HCl, pH 7.3, 1 mM EDTA) and incubated for 10 min. The reaction was initiated by adding 40 μL of a fluorogenic substrate (Dacyl-KTSAVLQSGFRKME-Edans) at a final concentration of 5 μM. After that, the fluorescence signal at 340 nm (excitation) and 490 nm (emission) was measured immediately every 1 min for 5 min with a Bio-Tek SynergyH1 plate reader. The velocities of reactions with compounds added at various concentrations compared to the reaction added with DMSO were calculated and used to generate inhibition profiles. For each compound, at least three biological replicates were performed for the determination of IC_{50} values.

4.10.2. Microsomal stability assay for **11b-11f** and **nirmatrelvir**

Preheat 100 mM K-buffer with 5 mM $MgCl_2$ to pH 7.41. Solutions of test and reference compounds were spiking. The tested concentration of compounds was 1 μM. NADPH stock solution (6 mM, 5 mg/mL) is prepared by dissolving NADPH in K/Mg-buffer. Dispense 30 μL of 1.5 μM spiking solution containing 0.75 mg/mL microsomes solution to the assay plates designated for different time points (0, 5, 15, 30, and 45 min). Pre-incubate the other plate at 37 °C for 5 min. For 0 min, add 150 μL of ACN containing IS to the wells before adding 15 μL of NADPH stock solution (6 mM). For other time points, add 15 μL of NADPH stock solution (6 mM) to the wells to start the reaction and timing. At 5 min, 15 min, 30 min, 45 min add 150 μL of ACN containing IS to the wells of corresponding plates, respectively, to stop the reaction. After quenching, shake the plates for 10 min (600 rpm) and then centrifuge at 6000 rpm for 15 min. Transfer 80 μL of the supernatant from each well into a 96-well sample plate containing 140 μL of pure water for LC/MS analysis.

4.10.3. Pharmacokinetics of **11b, 11e, 11j** and **nirmatrelvir**

All experiment procedures involving animals were in accordance with the guidelines of the Institutional Animal Care and Use Committee. The mice were randomly assigned into IV and PO groups, three mice per group. The mice received an intravenous (10 mg/kg) or oral (20 mg/kg) dose. After that, the whole blood samples were collected at 0.083 h, 0.25 h, 0.5 h, 1 h, 2 h, 4 h, 8 h and 24 h post-dose by intravenous administration. And the whole blood samples were collected at 0.25 h, 0.5 h, 1 h, 2 h, 4 h, 6 h, 8 h and 24 h post-dose by oral administration. An aliquot of a 20 μL plasma sample was protein precipitated with 400 μL MeOH, which contains 100 ng/mL IS. The mixture was vortexed for 1 min and centrifuged at 18000g for 10 min 400 μL of the supernatant should be transferred to 96-well plates. An aliquot of 8 μL supernatant was injected for LC-MS/MS analysis. The data analyzed and treated by the non-atrioventricular model, data acquisition and control system software were Phoenix WinNonlin 7.0 (Pharsight, USA).

4.10.4. Antiviral assay for **11e, 11j** and **nirmatrelvir**

Vero E6 cells (50000 cells/well) were plated into 48-well plates, and 200 μL/well medium containing 1 μM compound was added and incubated at 37 °C for 1 h. Then, SARS-CoV-2 WIV04 was added at a multiplicity of infection (MOI) of 0.01. After 24 h, the supernatant was collected, and the viral RNA was extracted from the supernatant. The viral copy number of the supernatant was detected by real-time fluorescence quantitative PCR. The inhibition rate of the compound was calculated based on the viral copy number.

4.10.5. Cytotoxic assay for **11e, 11j** and **nirmatrelvir**

Vero E6 cells were plated in the 384-well plates at a density of 2.5×10^3 cells per well for 48 h. Then the cells were incubated with the test articles at different concentrations (0.5–200 μM) for another 48 h ($n = 3$). A Luminescent Cell Viability Assay Kit purchased from Meilun Biotech Co., Ltd. (Dalian, China) was used for the cytotoxicity assay, with 10 μL of the Luminescent Cell Viability Assay Kit added to each well for 10 min. The absorbance was measured by an automatic microplate reader (Biotek, Winooski, VT, USA) at Luminescent. The half inhibitory concentration (IC_{50}) values for each compound were calculated by GraphPad Prism 8.3.0 software (GraphPad Software Inc., La Jolla, CA, USA).

4.10.6. Protease selectivity assay for **11j**

The chymotrypsin assay was performed as follows: Chymotrypsin (Sigma, catalog # SLCH1926) at a final concentration of 5 nM was mixed with 20 μM compound **11j** in an assay buffer (phosphate buffer saline, pH 7.4) and incubated for 10 min. Then, the fluorogenic substrate N-succinyl-AAPF-AMC at a final concentration of 10 μM was added to initiate the reaction. After that, the fluorescence signal was immediately measured at 380 nm (excitation) and 460 nm (emission) every 1 min for 10 min using a Bio-Tek Synergy-H1 plate reader.

The cathepsin B assay was performed in a reaction buffer containing 20 mM sodium acetate (pH 5.5), 1 mM EDTA, and 2 mM DTT. 0.25 units of cathepsin B (Sigma, catalog # SLCJ4379) and the testing compound **11j** were added to each well and incubated for 30 min at ambient temperature. The enzymatic reaction was started by adding 40 μL substrate (Z-RR-AMC) at a final concentration of 1 μM. After that, the fluorescence signal was immediately measured at 340 nm (excitation) and 440 nm (emission) every 1 min for 10 min with a Bio-Tek Synergy-H1 plate reader.

The cathepsin L (2 nM at a final concentration) was mixed with compound **11j** in 80 μL buffer (100 mM potassium phosphate, pH 6.8, 5 mM EDTA-Na, 0.001% Triton X-100, and 2 mM DDT). The reaction was initiated by adding 40 μL of the fluorogenic substrate Z-FR-AMC (20 μM). After that, the fluorescence signal was immediately measured at 360 nm (excitation) and 450 nm (emission) every 1 min for 10 min with a Bio-Tek Synergy-H1 plate reader.

Declaration of competing interest

The authors declare that they have no known competing financial interests or personal relationships that could have appeared to influence the work reported in this paper.

Data availability

Data will be made available on request.

Acknowledgment

This research was supported by National Key Research and Development Plan of China (2021YFC2300700 to L.K.Z., 2022YFC2303300 to L.K.Z.) and the Strategic Priority Research Program of Chinese Academy of Sciences (SIMM010120).

Appendix A. Supplementary data

Supplementary data to this article can be found online at https://doi.org/10.1016/j.ejmech.2023.115512.

Abbreviations

COVID-19	Coronavirus disease 2019
FDA	Food and Drug Administration
THF	tetrahydrofuran
Et_3N	triethylamine
DMF	*N*, *N*-dimethylformamide
AUC	area under the curve
EC_{50}	half-maximal effective concentration
DCM	dichloromethane
MeOH	methanol
PE	petroleum ether
TLC	thin layer chromatography
DMSO	dimethyl sulfoxide

References

[1] D.L. Tang, P. Comish, R. Kang, The hallmarks of COVID-19 disease, PLoS Pathog. 16 (2020) 1–24, https://doi.org/10.1371/journal.ppat.1008536.
[2] Y.J. Hao, Y.L. Wang, M.Y. Wang, L. Zhou, J.Y. Shi, J.M. Cao, D.P. Wang, The origins of COVID-19 pandemic: a brief overview, Transbound Emerg Dis 69 (2022) 3181–3197, https://doi.org/10.1111/tbed.14732.
[3] K.F. Gao, R. Wang, J.H. Chen, J. Tepe, F.Q. Huang, W. Guo, Perspectives on SARS-CoV-2 main protease inhibitors, J. Med. Chem. 64 (2021) 16922–16955, https://doi.org/10.1021/acs.jmedchem.1c00409.
[4] M.Y. Xiong, H.X. Su, W.F. Zhao, H. Xie, Q. Shao, Y.C. Xu, What coronavirus 3C-like protease tells us: from structure, substrate selectivity, to inhibitor design, Med. Res. Rev. 41 (2021) 1965–1998, https://doi.org/10.1002/med.21783.
[5] C.S. Dampalla, A.D. Rathnayake, K.D. Perera, A.R.M. Jesri, H.N. Nguyen, M. J. Miller, H.A. Thurman, J. Zheng, M.M. Kashipathy, K.P. Battaile, S. Lovell, S. Perlman, Y. Kim, W.C. Groutas, K.O. Chang, Structure-guided design of potent inhibitors of SARS-CoV-2 3CL protease: structural, biochemical, and cell-based studies, J. Med. Chem. 64 (2021) 17846–17865, https://doi.org/10.1021/acs.jmedchem.1c01037.
[6] C.S. Dampalla, Y. Kim, N. Bickmeier, A.D. Rathnayake, H.N. Nguyen, J. Zheng, M. M. Kashipathy, M.A. Baird, K.P. Battaile, S. Lovell, S. Perlman, K.O. Chang, W. C. Groutas, Structure-guided design of conformationally constrained cyclohexane inhibitors of severe acute respiratory syndrome Coronavirus-2 3CL protease, J. Med. Chem. 64 (2021) 10047–10058, https://doi.org/10.1021/acs.jmedchem.1c00319.
[7] H.X. Su, S. Yao, Zhao, W.F. Zhao, Y.M. Zhang, J. Liu, Q. Shao, Q.X. Wang, M.J. Li, H. Xie, W.J. Shang, C.Q. Ke, L. Feng, X.R. Jiang, J.S. Shen, G.F. Xiao, H.L. Jiang, L. K. Zhang, Y. Ye, Y.C. Xu, Identification of pyrogallol as a warhead in design of covalent inhibitors for the SARS-CoV-2 3CL protease, Nat. Commun. 12 (2021) 3623, https://doi.org/10.1038/s41467-021-23751-3.
[8] J.X. Qiao, Y.S. Li, R. Zeng, F.L. Liu, R.H. Luo, C. Huang, Y.F. Wang, J. Zhang, B. Quan, C.J. Shen, X. Mao, X.L. Liu, W.N. Sun, W. Yang, X.C. Ni, K. Wang, L. Xu, Z. L. Duan, Q.C. Zou, H.L. Zhang, W. Qu, Y.H.P. Long, M.H. Li, R.C. Yang, X.L. Liu, J. You, Y.L. Zhou, R. Yao, W.P. Li, J.M. Liu, P. Chen, Y. Liu, G.F. Lin, X. Yang, J. Zou, L.L. Li, Y.G. Hu, G.W. Lu, W. M Li, Y.Q. Wei, Y.T. Zheng, J. Lei, S.Y. Yang, SARS-CoV-2 M^{pro} inhibitors with antiviral activity in a transgenic mouse model, Science 371 (2021) 1374–1378. https://www.science.org/doi/10.1126/science.abf1611.
[9] K.S. Yang, S.Z. Leeuwon, S.Q. Xu, W.S.R. Liu, Evolutionary and structural insights about potential SARS-CoV-2 evasion of nirmatrelvir, J. Med. Chem. 65 (2022) 8686–8698, https://doi.org/10.1021/acs.jmedchem.2c00404.
[10] R. Cannalire, C. Cerchia, A.R. Beccari, F.S.D. Leva, V. Summa, Targeting SARS-CoV-2 proteases and polymerase for COVID-19 treatment: state of the art and future opportunities, J. Med. Chem. 65 (2022) 2716–2746, https://doi.org/10.1021/acs.jmedchem.0c01140.
[11] Y. Zhao, C. Fang, Q. Zhang, R.X. Zhang, X.B. Zhao, Y.K. Duan, H.F. Wang, Y. Zhu, L. Feng, J.Y. Zhao, M.L. Shao, X.N. Yang, L.K. Zhang, C. Peng, K.L. Yang, D.W. Ma, Z.H. Rao, H.T. Yang, Crystal structure of SARS-CoV-2 main protease in complex with protease inhibitor PF-07321332, Protein & Cell 13 (2022) 689–693, https://doi.org/10.1007/s13238-021-00883-2.
[12] S.H. Gao, L.T. Song, T. Claff, M. Woodson, K. Sylvester, L.L. Jing, R.H. Weiße, Y. S. Cheng, N. Sträter, L. Schäkel, M. Gütschow, B. Ye, M.L. Yang, T. Zhang, D. W. Kang, K. Toth, J. Tavis, A.E. Tollefson, C.E. Müller, P. Zhan, X.Y. Liu, Discovery and crystallographic studies of nonpeptidic piperazine derivatives as covalent SARS-CoV-2 main protease inhibitors, J. Med. Chem. 65 (2022) 16902–16917, https://doi.org/10.1021/acs.jmedchem.2c01716.
[13] Y. Hirose, N. Shindo, M. Mori, S. Onitsuka, H. Isogai, R. Hamada, T. Hiramoto, J. Ochi, D. Takahashi, T. Ueda, J.M.M. Caaveiro, Y. Yoshida, S. Ohdo, N. Matsunaga, S. Toba, M. Sasaki, Y. Orba, H. Sawa, A. Sato, E. Kawanishi, A. Ojida, Discovery of chlorofluoroacetamide-based covalent inhibitors for severe acute respiratory syndrome coronavirus 2 3CL protease, J. Med. Chem. 65 (2022) 13852–13865, https://doi.org/10.1021/acs.jmedchem.2c01716.
[14] X.Y.R. Ma, Y.R. Alugubelli, Y.Y. Ma, E.C. Vatansever, D.A. Scott, Y.C. Qiao, G. Yu, S.Q. Xu, W.S.R. Liu, MPI8 is potent against SARS-CoV-2 by inhibiting dually and selectively the SARS-CoV-2 main protease and the host cathepsinl, ChemMedChem 16 (2021) 1–9, https://doi.org/10.1002/cmdc.202100456.
[15] K.S. Yang, X.Y.R. Ma, Y.Y. Ma, Y.R. Alugubelli, D.A. Scott, E.C. Vatansever, A. K. Drelich, B. Sankaran, Z.Z. Geng, L.R. Blankenship, H.E. Ward, Y.J. Sheng, J. C. Hsu, K.C. Kratch, B.Y. Zhao, H.S. Hayatshahi, J. Liu, P.W. Li, C.A. Fierke, C.T. K. Tseng, S.Q. Xu, W.S.R. Liu, A Quick route to multiple highly potent SARS-CoV-2 main protease inhibitors, ChemMedChem 16 (2021) 942–948, https://doi.org/10.1002/cmdc.202000924.
[16] B. Bai, A. Belovodskiy, M. Hena, A.S. Kandadai, M.A. Joyce, H.A. Safffffran, J. A. Shields, M.B. Khan, E. Arutyunova, J. Lu, S.K. Bajwa, D. Hockman, C. Fischer, T. Lamer, W. Vuong, M.J. Belkum, Z.X. Gu, F. Lin, Y.H. Du, J. Xu, M. Rahim, H. S. Young, J.C. Vederas, D.L. Tyrrell, M.J. Lemieux, J.A. Nieman, Peptidomimetic α-acyloxymethylketone warheads with six membered lactam P1 glutamine mimic: SARS-CoV-2 3CL protease inhibition, coronavirus antiviral activity, and in vitro biological stability, J. Med. Chem. 65 (2022) 2905–2925, https://doi.org/10.1021/acs.jmedchem.1c00616.
[17] R. Banerjee, L. Perera, L.M.V. Tillekeratne, Potential SARS-CoV-2 main protease inhibitors, Drug Discov. Today 26 (2021) 804–816, https://doi.org/10.1016/j.drudis.2020.12.005.
[18] W. Vuong, M.B. Khan, C. Fischer, E. Arutyunova, T. Lamer, J. Shields, H.A. Saffran, R.T. McKay, M.J. Belkum, M.A. Joyce, H.S. Young, D.L. Tyrrell, J.C. Vederas, M. J. Lemieux, Feline coronavirus drug inhibits the main protease of SARS-CoV-2 and blocks virus replication, Nat. Commun. 11 (2020) 4282, https://doi.org/10.1038/s41467-020-18096-2.
[19] L.F. Fu, F. Ye, Y. Feng, F. Yu, Q.S. Wang, Y. Wu, C. Zhao, H. Sun, B.Y. Huang, P. H. Niu, H. Song, Y. Shi, X.B. Li, W.J. Tan, J.X. Qi, G.F. Gao, Both Boceprevir and GC376 efficaciously inhibit SARS-CoV-2 by targeting its main protease, Nat. Commun. 11 (2020) 4417, https://doi.org/10.1038/s41467-020-18233-x.
[20] B. Boras, R.M. Jones, B.J. Anson, D. Arenson, L. Aschenbrenner, M.A. Bakowski, N. Beutler, J. Binder, E. Chen, H. Eng, J. Hammond, R. Hoffman, E.P. Kadar, R. Kania, E. Kimoto, M.G. Kirkpatrick, L. Lanyon, E.K. Lendy, J.R. Lillis, S. A. Luthra, C. Ma, S. Noell, R.S. Obach, M.N. O'Brien, R. O'Connor, K. Ogilvie, D. Owen, M. Pettersson, M.R. Reese, T.F. Rogers, M.I. Rossulek, J.G. Sathish, C. Steppan, M. Ticehurst, L.W. Updyke, Y. Zhu, J. Wang, A.K. Chatterjee, A. D. Mesecar, A.S. Anderson, C. Allerton, Preclinical characterization of an intravenous coronavirus 3CL protease inhibitor for the potential treatment of COVID-19, Nat. Commun. 12 (2021) 6055, https://doi.org/10.1038/s41467-021-26239-2.
[21] S. Ullrich, C. Nitsche, The SARS-CoV-2 main protease as drug target, Bioorg. Med. Chem. Lett. 30 (2020), 127377, https://doi.org/10.1016/j.bmcl.2020.127377.
[22] D.R. Owen, C.M.N. Allerton, A.S. Anderson, L. Aschenbrenner, M. Avery, S. Berritt, B. Boras, R.D. Cardin, A. Carlo, K.J. Coffman, A. Dantonio, L. Di, H. Eng, R.A. Ferre, K.S. Gajiwala, S.A. Gibson, S.E. Greasley, B.L. Hurst, E.P. Kadar, A.S. Kalgutkar, J. C. Lee, J. Lee, W. Liu, S.W. Mason, S. Noell, J.J. Novak, R.S. Obach, K. Ogilvie, N. C. Patel, M. Pettersson, D.K. Rai, M.R. Reese, M.F. Sammons, J.G. Sathish, R.S. P. Singh, C.M. Steppan, A.E. Stewart, J.B. Tuttle, L. Updyke, P.R. Verhoest, L. Q. Wei, Q.Y. Yang, Y. Zhu, An oral SARS-CoV-2 M^{pro} inhibitor clinical candidate for the treatment of COVID-19, Science 374 (2021) 1586–1593. https://www.science.org/doi/10.1126/science.abl4784.
[23] Y.N. Lamb, Nirmatrelvir plus ritonavir: first approval, Drugs 82 (2022) 585–591, https://doi.org/10.1007/s40265-022-01692-5.
[24] M. Sindelar, D. McCabe, E. Carroll, Tacrolimus drug-drug interaction with nirmatrelvir/ritonavir (Paxlovid) managed with phenytoin, J. Med. Toxicol. 19 (2023) 45–48, https://doi.org/10.1007/s13181-022-00922-2.
[25] C. Marzolini, D.R. Kuritzkes, F. Marra, A. Boyle, S. Gibbons, C. Flexner, A. Pozniak, M. Boffito, L. Waters, D. Burger, D.J. Back, S. Khoo, Recommendations for the management of drug-drug interactions between the COVID-19 antiviral nirmatrelvir/ritonavir (Paxlovid) and comedications, Clin. Pharmacol. Ther. 112 (2022) 1191–1200, https://doi.org/10.1002/cpt.2646.
[26] H.H. Yang, J.F. Yang, A review of the latest research on M^{pro} targeting SARS-COV inhibitors, RSC Med Chem 12 (2021) 1026–1036, https://doi.org/10.1039/D1MD00066G.
[27] J.K. Stille, J. Tjutrins, G.Y. Wang, F.A. Venegas, C. Hennecker, A.M. Rueda, I. Sharon, N. Blaine, C.E. Miron, P. S, A. Labarre, J. Plescia, M.B. Patrascu, X. C. Zhang, A.S. Wahba, D. Vlaho, M.J. Huot, T.M. Schmeing, A.K. Mittermaier, N. Moitessier, Design, synthesis and in vitro evaluation of novel SARS-CoV-2 $3CL^{pro}$ covalent inhibitors, Eur. J. Med. Chem. 229 (2022), 114046, https://doi.org/10.1016/j.ejmech.2021.114046.
[28] S.H. Gao, K. Sylvester, L.T. Song, T. Claff, L.L. Jing, M. Woodson, R.H. Weiße, Y. S. Cheng, L. Schäkel, M. Petry, M. Gütschow, A.C. Schiedel, N. Sträter, D.W. Kang, S.J. Xu, K. Toth, J. Tavis, A.E. Tollefson, C.E. Müller, X.Y. Liu, P. Zhan, Discovery and crystallographic studies of trisubstituted piperazine derivatives as non-

covalent SARS-CoV-2 main protease inhibitors with high target specificity and low toxicity, J. Med. Chem. 65 (2022) 13343–13364, https://doi.org/10.1021/acs.jmedchem.2c01146.

[29] J. Breidenbach, C. Lemke, T. Pillaiyar, L. Schäkel, G.A. Hamwi, M. Diett, R. Gedschold, N. Geiger, V. Lopez, S. Mirza, V. Namasivayam, A.C. Schiedel, K. Sylvester, D. Thimm, C. Vielmuth, L.P. Vu, M. Zyulina, J. Bodem, M. Gütschow, C.E. Müller, Targeting the main protease of SARS-CoV-2: from the establishment of high throughput screening to the design of tailored inhibitors, Angew. Chem., Int. Ed. Engl. 60 (2021) 10423–10429, https://doi.org/10.1002/anie.202016961.

[30] R.F. Chen, Y.L. Gao, H. Liu, H. Li, W.F. Chen, J.J. Ma, Advances in research on 3C-like protease ($3CL^{pro}$) inhibitors against SARS-CoV-2 since 2020, RSC Med. Chem. 14 (2023) 9–21, https://doi.org/10.1039/D2MD00344A.

[31] W.H. Dai, B. Zhang, X.M. Jiang, H.X. Su, J. Li, Y. Zhao, X. Xie, Z.M. Jin, J.J. Peng, F.J. Liu, C. Li, Y. Li, F. Bai, H.F. Wang, X. Cheng, X.B. Cen, S.L. Hu, X.N. Yang, J. Wang, X. Liu, G.F. Xiao, H.L. Jiang, Z.H. Rao, L.K. Zhang, Y.C. Xu, H.T. Yang, H. Liu, Structure-based design of antiviral drug candidates targeting the SARS-CoV-2 main protease, Science 368 (2020) 1331–1335. https://www.science.org/doi/10.1126/science.abb4489.

[32] W. Vuong, C. Fischer, M.B. Khan, M.J. van Belkum, T. Lamer, K.D. Willoughby, J. Lu, E. Arutyunova, M.A. Joyce, H.A. Saffran, J.A. Shields, H.S. Young, J. A. Nieman, D.L. Tyrrell, M.J. Lemieux, J.C. Vederas, Improved SARS-CoV-2 M^{pro} inhibitors based on feline antiviral drug GC376: structural enhancements, increased solubility, and micellar studies, Eur. J. Med. Chem. 222 (2021), 113584, https://doi.org/10.1016/j.ejmech.2021.113584.

[33] A. Citarella, A. Scala, A. Piperno, N. Micale, SARS-CoV-2 M^{pro}: a potential target for peptidomimetics and small-molecule inhibitors, Biomolecules 11 (2021) 607, https://doi.org/10.3390/biom 11040607.

[34] L.L. Zhang, D.Z. Lin, X.Y.Y. Sun, U. Curth, C. Drosten, L. Sauerhering, S. Becker, K. Rox, R. Hilgenfeid, Crystal structure of SARS-CoV-2 main protease provides a basis for design of improved a-ketoamide inhibitors, Science 368 (2020) 409–412. https://www.science.org/doi/10.1126/science.abb3405.

[35] Z.M. Jin, X.Y. Du, Y.C. Xu, Y.Q. Deng, M.Q. Liu, Y. Zhao, B. Zhang, X.F. Li, L. K. Zhang, C. Peng, Y.K. Duan, J. Yu, L. Wang, K.L. Yang, F.J. Liu, R.D. Jiang, X. L. Yang, T. You, X.C. Liu, X.N. Yang, F. Bai, H. Liu, X. Liu, L.K.W. Guddat, W.Q. Xu, G.F. Xiao, C.F. Qin, Z.L. Shi, H.L. Jiang, Z.H. Rao, H.T. Yang, Structure of M^{pro} from SARS-CoV-2 and discovery of its inhibitors, Nature 582 (2020) 289–293, https://doi.org/10.1038/s41586-020-2223-y.

[36] R.L. Hoffman, R.S. Kania, M.A. Brothers, J.F. Davies, R.A. Ferre, K.S. Gajiwala, M. Y. He, R.J. Hogan, K. Kozminski, L.L.Y. Li, J.W. Lockner, J.H. Lou, M.T. Marra, L. J. Mitchell, B.W. Murray, J.A. Nieman, S. Noell, S.P. Planken, T. Rowe, K. Ryan, G. J. Smith, J.E. Solowiej, C.M. Steppan, B. Taggart, Discovery of ketone-based covalent inhibitors of coronavirus 3CL proteases for the potential therapeutic treatment of COVID-19, J. Med. Chem. 63 (2020) 12725–12747, https://doi.org/10.1021/acs.jmedchem.0c01063.

[37] S. Konno, P. Thanigaimalai, T. Yamamoto, K. Nakada, R. Kakiuchi, K. Takayama, Y. Yamazaki, F. Yakushiji, K. Akaji, Y. Kiso, Y. Kawasaki, S.E. Chen, E. Freire, Y. Hayashi, Design and synthesis of new tripeptide-type SARS-CoV 3CL protease inhibitors containing an electrophilic arylketone moiety, Bioorg. Med. Chem. 21 (2013) 412–424, https://doi.org/10.1016/j.bmc.2012.11.017.

[38] P. Thanigaimalai, S. Konno, T. Yamamoto, Design, synthesis, and biological evaluation of novel dipeptide-type SARS-CoV 3CL protease inhibitors: structure-activity relationship, Eur. J. Med. Chem. 65 (2013) 436–447, https://doi.org/10.1021/acs.jmedchem.0c01063.

[39] P. Thanigaimalai, S. Konno, T. Yamamoto, Y. Koiwai, A. Taguchi, K. Takayama, F. Yakushiji, K. Akaji, S.E. Chen, A.N. Tavakolian, A. Schön, E. Freire, Y. Hayashi, Development of potent dipeptide-type SARS-CoV 3CL protease inhibitors with novel P3 scaffolds: design, synthesis, biological evaluation, and docking studies, Eur. J. Med. Chem. 68 (2013) 372–384, https://doi.org/10.1016/j.ejmech.2013.07.037.

[40] S. Konno, K. Kobayashi, M. Senda, Y. Funai, Y. Seki, I. Tamai, L. Schäkel, K. Sakata, T. Pillaiya, A. Taguchi, A. Taniguchi, M. Gütschow, C.E. Müller, K. Takeuchi, M. Hirohama, A. Kawaguchi, M. Kojima, T. Senda, Y. Shirasaka, W. Kamitani, Y. Hayashi, 3CL protease inhibitors with an electrophilic arylketone moiety as anti-SARS-CoV-2 agents, J. Med. Chem. 65 (2022) 2926–2939, https://doi.org/10.1021/acs.jmedchem.1c00665.

[41] D.W. Kneller, H. Li, G. Phillips, K.L. Weiss, Q. Zhang, M.A. Arnould, C.B. Jonsson, S. Surendranathan, J. Parvathareddy, M.P. Blakeley, L. Coates, J. M Louis, P. V. Bonnesen, A. Kovalevsky, Covalent narlaprevir- and boceprevir-derived hybrid inhibitors of SARS-CoV-2 main protease, Nat. Commun. 13 (2022) 2268, https://doi.org/10.1038/s41467-022-29915-z.

[42] J.O. Link, J.G. Taylor, L.H. Xu, M. Mitchell, H.Y. Guo, H.T. Liu, D. Kato, T. Kirschberg, J.Y. Sun, N. Squires, J. Parrish, T. Kellar, Z.Y. Yang, C. Yang, M. Matles, Y.J. Wang, K. Wang, G.F. Cheng, Y. Tian, E. Mogalian, E. Mondou, M. Cornpropst, J. Perry, M.C. Desai, Discovery of Ledipasvir (GS-5885): a potent, once-daily oral NS5A inhibitor for the treatment of hepatitis C virus infection, J. Med. Chem. 57 (2014) 2033–2046, https://doi.org/10.1021/jm401499g.

[43] S. Iketani, F. Forouhar, H.R. Liu, S.J. Hong, F.Y. Lin, M.S. Nair, A. Zask, Y. X. Huang, L. Xing, B.R. Stockwell, A. Chavez, D.D. Ho, Lead compounds for the development of SARS-CoV-2 3CL protease inhibitors, Nat. Commun. 12 (2021) 2016, https://doi.org/10.1038/s41467-021-22362-2.

[44] H.R. Liu, S. Iketani, A. Zask, N. Khanizeman, E. Bednarova, F. Forouhar, B. Fowler, S.J. Hong, H. Mohri, M.S. Nair, Y.X. Huang, N.E.S. Tay, S. Lee, C. Karan, S. J. Resnick, C. Quinn, W.J. Li, H. Shion, X. Xia, J.D. Daniels, M.B. Cruz, M. Farina, P. Rajbhandari, C. Jurtschenko, M.A. Lauber, T.M. Donald, M.E. Stokes, B.L. Hurst, T. Rovis, A. Chavez, D.D. Ho, B.R. Stockwell, Development of optimized drug-like small molecule inhibitors of the SARS-CoV-2 3CL protease for treatment of COVID-19, Nat. Commun. 13 (2022) 1891, https://doi.org/10.1038/s41467-022-29413-2.

[45] R. Hilgenfeld, From SARS to MERS: crystallographic studies on coronaviral proteases enable antiviral drug design, FEBS J. 281 (2014) 4085–4096, https://doi.org/10.1111/febs.12936.